Published in final edited form as:
Nat Rev Nephrol. 2021 October 01; 17(10): 688–703. doi:10.1038/s41581-021-00440-4.

Non-invasive molecular imaging of kidney diseases

Barbara M. Klinkhammer[1], **Twan Lammers**[2,3,4], **Felix M. Mottaghy**[5,6], **Fabian Kiessling**[2,7], **Jürgen Floege**[8], **Peter Boor**[1,8,9,†]

[1]Institute of Pathology, RWTH Aachen University Hospital, Aachen, Germany

[2]Institute for Experimental Molecular Imaging, RWTH Aachen University Hospital, Aachen, Germany

[3]Department of Pharmaceutics, Utrecht University, The Netherlands

[4]Department of Targeted Therapeutics, University of Twente, Enschede, The Netherlands

[5]Department of Nuclear Medicine, University Hospital RWTH Aachen, Germany

[6]Department of Radiology and Nuclear Medicine, Maastricht University Medical Center, Maastricht, the Netherlands

[7]Fraunhofer Institute for Digital Medicine MEVIS, Bremen, Germany

[8]Department of Nephrology and Immunology, RWTH Aachen University Hospital, Aachen, Germany

[9]Electron Microscopy Facility, RWTH Aachen University Hospital, Aachen, Germany

Abstract

In nephrology, differential diagnosis or assessment of disease activity largely relies on the analysis of glomerular filtration rate, urinary sediment, proteinuria and tissue obtained through invasive kidney biopsies. However, currently available non-invasive functional parameters, and most serum and urine biomarkers cannot capture intrarenal molecular disease processes specifically. Moreover, although histopathological analyses of kidney biopsy samples enable the visualization of pathological morphological and molecular alterations, they only provide information on a small part of the kidney and do not allow longitudinal monitoring. These limitations not only hinder understanding of the dynamics of specific disease processes in the kidney, but also limit the targeting of treatments to active phases of disease and the development of novel targeted therapies. Molecular imaging enables non-invasive and quantitative assessment of physiological

† pboor@ukaachen.de .

Author contributions

All authors made substantial contributions to discussions of the manuscript content. B.M.K. researched the data for the article and wrote the first draft of the manuscript. T.L., F.M.M., F.K., J.F. and P.B. reviewed and edited the manuscript before submission.

Competing interests

F.M.M. is an advisory board member for Advanced Accelerator Applications/Novartis and Bayer, holds speaker positions at Siemens, GE Healthcare and Bayer, and receives institutional grants from GE Healthcare and Nanomab. F.K. consults for Merck Darmstadt, holds patents and has running patent applications with Bayer, Roche and Visualsonics, has stock options for Molecular Targeting Inc. and co-owns InVivoContrast GmbH. The remaining authors declare no competing interests.

Peer review information

TBC

Europe PMC Funders Author Manuscripts

or pathological processes by combining imaging technologies with specific molecular probes. Here, we discuss current preclinical and clinical molecular imaging approaches in nephrology. Molecular imaging enables non-invasive visualization of the kidneys, and helps to detect and longitudinally monitor disease activity. These approaches can also provide companion diagnostics to guide clinical trials, as well as the safe and effective use of drugs.

Europe PMC Funders Author Manuscripts

Introduction

Molecular imaging employs tools and technologies that enable the visualization and quantification of chemical and biological processes in living organisms. To address the inconsistent use of the broad term ‘molecular imaging’, in 2005, a molecular imaging summit organized by the Radiological Society of North America (RSNA) and the Society of Nuclear Medicine and Molecular Imaging (SNMMI), defined that “molecular imaging techniques directly or indirectly monitor and record the spatiotemporal distribution of molecular or cellular processes for biochemical, biologic, diagnostic, or therapeutic applications”[1]. In 2007, the definition of molecular imaging was further refined to “the visualization, characterization, and measurement of biological processes at the molecular and cellular levels in humans and other living systems”[2]. Here, we will explicitly focus on *in vivo* non-invasive molecular imaging approaches, including nuclear molecular imaging (positron emission tomography (PET) or single-photon emission computed tomography (SPECT)), ultrasound, magnetic resonance imaging (MRI) and optical imaging. These approaches require the use of molecular probes (also known as molecular imaging agents), which are compounds that specifically bind to (or are transported or activated by) molecules involved in a biological or disease-relevant pathway. These probes — small molecules, peptides, antibodies, nanobodies **[G]**, aptamers **[G]** or nanoparticles — are functionally modified to serve as contrast agents, radiolabeled tracers or fluorescence-emitting agents depending on the imaging technique. Nearly all of these probes can be radiolabeled directly, *via* linkers or chelators, for use in nuclear molecular imaging. Other molecular imaging agents include antibody- or peptide-functionalized microbubbles **[G]** that are used for ultrasound imaging of vascular receptors, antibody-modified iron oxide nanoparticles that bind to receptors overexpressed by cancer cells and can be used in MRI, and target-specific fluorescent dyes that are used in optical imaging applications, including fluorescence molecular tomography (FMT) and optical surgical navigation (OSN). With respect to molecular imaging in kidney diseases, each modality has its own advantages and disadvantages (Table 1).

Non-invasive molecular imaging is a valuable and increasingly used diagnostic tool, in particular in oncology[3,4], neurology[5] and cardiology[6,7]. In oncology, molecular imaging is widely recognized as a support tool in precision medicine (that is, individualized treatment based on specific patient and disease characteristics). As in the field of oncology[4], molecular imaging might also enable precision nephrology through its application to four key areas of clinical research: identification of therapeutic targets and selection of patients who might benefit from therapy (that is, companion diagnostics); measurement of drug pharmacokinetics and drug delivery, as well as optimization of drug dosing; measurement of drug effects and therapeutic responses; and prediction of patient outcomes (Figure 1).

However, in contrast to oncology, the use of molecular imaging approaches in nephrology is still limited.

In this Review, we discuss current preclinical and clinical applications of non-invasive molecular imaging in nephrology, such as experimental elastin-targeted MRI in fibrosis, clinical [^{18}F]FDG(2-deoxy-2-[18F]fluoroglucose)-PET for inflammation or carbonic anhydrase 9 (CA9; also known as CAIX)-targeted PET in renal cell carcinoma (RCC), with a focus on major pathological processes and kidney diseases. We also examine the challenges of applying molecular imaging to kidney diseases.

Tubular damage and acute kidney injury

Several studies of molecular imaging in the kidney have focused on tubular injury and acute kidney injury (AKI). A group of clinical radiopharmaceuticals can be used to measure kidney function by providing information on the activity of different tubular transporters (Table 2). These probes include several ^{99m}Tc-labeled compounds — dimercaptosuccinic acid (DMSA), mercaptoacetyltriglycine (MAG3), ethylenedicysteine (EC), para-aminohippuric acid (PAH) and tricarbonyl-labeled (CO3) nitrilotriacetic acid (NTA). Of note, ^{131}I-labeled and ^{123}I-labeled orthoiodohippurate (OIH)[8–12] are no longer used in clinical practice because they lead to relatively high radiation exposure.

Changes in tubular epithelium function

^{99m}Tc-DMSA is freely filtered in the glomerulus but ~40% of the injected dose is retained in the kidney proximal tubules within 1 h of injection[8]. This compound binds to the plasma protein α1-microglobulin, which is a ligand for the megalin and cubilin receptors. Whole-body scintigrams of mice deficient for megalin or cubilin showed an almost complete absence of ^{99m}Tc-DMSA tubular reabsorption[13]. ^{99m}Tc-DMSA uptake in the kidneys of patients with proximal tubule disorders characterized by a defect in endocytosis mediated by megalin and/or cubilin, such as Dent disease or Lowe syndrome, was lower than in patients with functional receptors, which further confirmed the findings in mice[14]. Hence, ^{99m}Tc-DMSA accumulation in the kidney is dependent on megalin and/or cubilin-mediated endocytosis and can be used as a marker of endocytic activity in the proximal tubule. Imaging with ^{99m}Tc-DMSA has been used to detect several diseases, including pyelonephritis, nephrolithiasis or hydronephrosis, and to assess kidney dysfunction in experimental models of kidney disease such as gentamycin-induced nephropathy, adenine-induced nephropathy or unilateral ureteral obstruction. However, the renal uptake of ^{99m}Tc-DMSA not only depends on proximal tubule receptor-mediated endocytosis, but is also affected by renal blood flow and glomerular filtration, and cannot therefore be used to assess tubular physiology specifically[15–17]. A similar limitation applies to imaging with PAH and OIH. Both of these compounds enable the estimation of effective renal plasma flow because they have high plasma clearance, which is mostly driven by their uptake into proximal tubules *via* organic anion transporter 1 (OAT1; encoded by *SLC22A6*) and OAT3 (encoded by *SLC22A8*), followed by secretion into the lumen; however, ~25% of the excretion of these compounds occurs through glomerular filtration.

^{99m}Tc-MAG3 is an attractive probe owing to its high extraction efficiency **[G]** and has replaced ^{131}I-OIH and ^{123}I-OIH in clinical practice for the evaluation of single-kidney tubular extraction, perfusion and clearance, not only because it reduces radiation exposure but also because it is more widely available and easier to prepare with a simple kit. Physiologically, ^{99m}Tc-MAG3 is exclusively secreted from peritubular capillaries into tubular cells *via* basolateral OATs expressed in the proximal convoluted tubules, and further transported from tubular cells into the lumen *via* multidrug resistance-associated protein 2 (encoded by *ABCC2)* in the luminal membrane[18]. The parenchymal transit of ^{99m}Tc-MAG3 is delayed following kidney damage (especially tubular damage), which results in persistent probe activity in the renal parenchyma and delayed radiotracer detection in the pelvis and bladder. Consequently, ^{99m}Tc-MAG3 is primarily used to measure function and damage in a single kidney, for example in cases of hydronephrosis[19] or ischaemia[20].

^{99m}Tc-probestin is a high affinity ligand and inhibitor of the aminopeptidase N (APN) enzyme, which is highly expressed in proximal tubule epithelial cells[21]. SPECT imaging of mice injected with ^{99m}Tc-probestin showed high accumulation of the probe in the kidney cortex in wild-type mice, whereas probe uptake was reduced in UPII-SV40T transgenic mice, which express SV40 under the control of the uroplakin 2 promotor and develop an invasive transitional cell carcinoma that invades the kidneys and replaces the normal parenchyma[21].

Injury biomarkers and processes

All the approaches mentioned above monitor kidney damage indirectly by detecting alterations in tubular epithelial cell function. Alternatively, tubular injury can be assessed by targeting injury biomarkers or processes. Iopamidol, for example, is a pH-responsive chemical exchange saturation transfer (CEST)–MRI contrast agent that has been used in mice to image the pH of the kidney parenchyma in AKI models. Mice with rhabdomyolysis[22] or ischaemia-induced[23] AKI not only had reduced kidney perfusion, but their kidney pH was also markedly increased compared with controls owing to tubular cell death and dysregulation of pH homeostasis.

Tubular cell damage and necrotic cell death have also been imaged by MRI in mice using hyperpolarized [1,4-$^{13}C_2$]fumarate[24]. Fumarate hydratase contributes to the mitochondrial tricarboxylic acid cycle by converting fumarate to malate and, under physiological conditions, this enzymatic activity is restricted to the intracellular environment. However, following cell necrosis, the presence of free fumarate hydratase in serum enables the conversion of [1,4-$^{13}C_2$]fumarate to [1,4-^{13}C2]malate, which can therefore be used as a marker of necrotic cell death. In two models of acute tubular necrosis — ischaemia-reperfusion injury and folic acid-induced nephropathy — [1,4-$^{13}C_2$]malate in the kidney increased significantly compared with controls and this increase preceded severe histolopathological cell damage[24,25]. Of note, such an increase was not observed in a model of lupus nephritis (NZM2410 mice) that is not characterized by necrotic tubular cell death[24,25]. This technique was suggested as a tool to identify a window of therapeutic opportunity for emerging therapies that prevent cell death[24]. Another interesting option would be to test this approach for imaging of treatment responses in kidney cancer —

[1,4-$^{13}C_2$] fumarate imaging seemed suitable for in vivo detection of tumor cell death in mice with lymphoma after chemotherapeutic treatment with etoposide[26].

The use of optical near-infrared fluorescence (NIRF) for imaging kidney oxidative stress, lysosomal damage and apoptosis has also yielded promising results in preclinical models[27]. Mice with AKI induced by cisplatin, gentamycin or diatrizoate were injected with non-toxic molecular kidney probes, including compounds that targeted superoxide anions to detect oxidative stress, *N*-acetyl-β-D-glucosaminidase as a marker of lysosomal damage, and caspase-3 as a marker for apoptosis. Longitudinal imaging showed that all three pathological processes occurred sequentially after exposure to nephrotoxins[27]. Most importantly, all three events preceded the clinical manifestation of AKI, including a decrease in glomerular filtration rate (GFR) and the presence of urinary damage markers such as neutrophil gelatinase-associated lipocalin (NGAL), cystatin C or β2-microglobulin[27,28]. This imaging approach might therefore enable AKI detection earlier than existing clinical parameters, which might improve AKI management.

In addition to tubular injury, endothelial damage can be both a trigger and an imaging hallmark of AKI. MRI or ultrasound imaging studies have focused on imaging P-selectin (CD62P) and vascular cell adhesion molecule 1 (VCAM1), both of which are upregulated in injured endothelial cells and serve as injury biomarkers[29,30] (Fig. 2). VCAM1, which is a receptor for α4β1 integrin and has an important role in leukocyte recruitment, is expressed and upregulated on endothelial cells after ischaemic injury. After injection of VCAM1-targeting microparticles of iron oxide (MPIO) into mice with ischaemia-induced AKI, kidney MRI signals were markedly changed and correlated with tissue *Vcam1* mRNA expression[29]. Binding of the probes in kidneys occurred rapidly after injection and unbound MPIO were actively sequestered in the liver and spleen[29]. VCAM1 and P-selectin were also targeted *via* antibody-functionalized microbubbles for molecular ultrasound imaging[30]. In rats and in mice with IRI, imaging signals for both targets were markedly increased at 2h, 4h and 24h, and correlated with target protein expression in the kidneys[30–32].

When imaging endothelial targets, ultrasound is advantageous because its probes remain strictly in the intravascular space and the imaging does not depend directly on GFR. Another advantage is that ultrasound imaging is cheap and ultrasound devices are broadly available. If ultrasound molecular probes become available commercially in future, molecular ultrasound in kidneys might be readily translated into human application. Moreover, considering that imaging of endothelial damage and angiogenesis has been intensively explored for many diseases and organs, probes developed, for example, for use in cardiovascular or neoplastic diseases, might be potentially applied to nephrology[33,34].

Inflammation

Imaging of inflammatory processes might involve targeting immune cells, pro-inflammatory signaling molecules or the complement system (Fig. 2, Table 2). Imaging of glucose metabolism using PET and the molecular probe ^{18}F-fluoro-2-deoxyglucose (^{18}F-FDG) is the only approach to image inflammation currently established in the clinic but it does not target inflammatory cells specifically. In cells with high glucose metabolism,

^{18}F-FDG is taken up *via* glucose transporters (GLUT), phosphorylated by hexokinase and retained within the cell. ^{18}F-FDG-PET therefore reflects glucose tissue uptake and metabolism, and is used extensively to visualize malignancies and inflammatory diseases. Activated inflammatory cells, such as macrophages, lymphocytes and neutrophils, consume high amounts of glucose and therefore accumulate ^{18}F-FDG efficiently. In patients with pyelonephritis, two patterns of uptake were associated with distinct clinical presentations — a diffuse pattern of ^{18}F-FDG was observed in cases without severe fever and with atypical symptoms such as abdominal, suprapubic and/or periumbilical pain, whereas patients with a focal pattern frequently required prolonged antibiotic therapy and hospital stays[35]. In another small retrospective single-centre study, ^{18}F-FDG-PET imaging had a sensitivity of 89%, a specificity of 75%, a positive predictive value of 84%, and a negative predictive value of 82% for the diagnosis of cyst infection in patients with autosomal dominant polycystic kidney disease (ADPKD)[36]. An additional trial tested the use of ^{18}F-FDG-PET scans in 104 patients receiving haemodialysis and reported that this approach could be used to detect infection foci and assess mortality risk in this cohort[37].

In all of these kidney diseases with an inflammatory component, ^{18}F-FDG-PET imaging demonstrated potential to identify patients with a poor prognosis. However, because this approach is not sufficiently specific for inflammation, its usefulness beyond very specific cohorts or questions remains unclear. More specific probes and targets that can support therapy decisions would therefore be very helpful. Some candidates that detect different types of immune cells have been identified in the context of kidney transplant rejection (discussed below) and might be applicable to other settings of non-transplant-associated kidney inflammation[38–42].

Probes can also target the complement system. Glomerular complement C3 fragments were imaged through MRI in MRL/lpr mice with lupus nephritis[43] using superparamagnetic iron oxide (SPIO). The C3 probe was generated by synthesizing a recombinant protein containing the C3d-binding region of complement receptor type 2 conjugated to the surface of SPIO nanoparticles[43,44]. Mice were imaged at 12, 16, 20 and 24 weeks of age and not only showed significant changes in signals compared with healthy controls, but also had a significant signal change at 20 weeks compared with earlier ages, indicating that imaging of disease progression is feasible[43]. Another study used MRI to detect C5b-9 in rats with Heymann nephritis by injecting anti-C5b-9 antibodies conjugated to USPIO[45]. Signal intensities changed significantly in the kidneys 24 hours after probe injection compared with either healthy animals or diseased animals injected with control IgG. Signal specificity was confirmed *ex vivo* by detecting nanoparticle deposits in diseased glomeruli through electron microscopy[45]. Such complement imaging protocols would be of high interest in nephrology, given the crucial involvement of complement in many kidney diseases and the various complement-targeted therapies available[46]. Whether these imaging approaches can be transferred to the clinic, for example, for use in patients with lupus nephritis or thrombotic microangiopathy, remains to be tested.

Europe PMC Funders Author Manuscripts

Kidney transplant rejection

Although short-term outcomes after kidney transplantation have improved significantly over the past few decades, the lack of organ availability and poor long-term outcomes remain important challenges. Currently, kidney biopsy is the gold standard for detection of rejection or chronic allograft nephropathy, but some non-invasive (non-molecular) imaging approaches that use ultrasound, computed tomography (CT) and MRI to detect changes, for example, in kidney perfusion and blood flow, are potentially useful (reviewed in[47]).

Nuclear molecular imaging approaches, including the use of ^{18}F-FDG (REF.[48]), ^{99m}Tc-DMSA (REF.[49]) or ^{99m}Tc-MAG3 (REF.[50]), have been implemented in some national guidelines for quantitative detection of kidney allograft rejection and can be used for early prediction of acute transplant rejection[51,52]. Both ^{99m}Tc-based imaging approaches focus on tubular function and parenchymal transport, as well as perfusion, integrity of vascular supply and post-renal obstruction. Older clinical approaches included scintigraphy using ^{99m}Tc-sulfur colloids, ^{131}I-fibringogen or ^{125}I-fibringogen to detect fibrin thrombosis, and ^{67}Ga-citrate to detect granulocytes in transplanted kidneys[38,53–55]. ^{99m}Tc-sulfur colloids were useful for the detection of acute and chronic rejection because these types of rejection resulted in high radiocolloid accumulation, whereas radioactive signals were low or absent in patients with normal transplant function or acute tubular necrosis[38,54]. However, none of these radiopharmaceuticals are currently commercially available and are therefore not routinely used in the clinic.

A prospective study using ^{18}F-FDG-PET in 31 transplant recipients showed a positive correlation between signal intensity and the Banff score **[G]**, but could not identify the cause of graft inflammation and dysfunction because, as described above, ^{18}F-FDG-based imaging reflects glucose metabolism and therefore does not provide specific information on the cause or type of rejection. Data analysis revealed that for a mean standardized uptake value **[G]** (SUV) threshold of 1.6, the sensitivity and specificity of ^{18}F-FDG–PET imaging for diagnosing acute rejection were 100% and 50%, respectively[48]. A follow-up observational clinical trial is currently recruiting patients and aims to assess the usefulness of ^{18}F-FDG-PET–CT for predicting allograft survival in kidney transplant recipients (NCT03764124; Table 3).

Several alternative approaches focus on the discrimination between humoral or cell-mediated rejection, and the detection of tubular necrosis. One preclinical study aimed to detect humoral rejection using C4d-targeted microbubbles for ultrasound molecular imaging of rats with allogeneic kidney transplants[56]. The ultrasound signals showed a very high and almost linear correlation with the extent of C4d$^+$ peritubular capillaries. This imaging approach did not affect the survival rates or kidney pathology, suggesting that it might be feasible and safe[56].

In a rat model of allogeneic transplantation, adoptive transfer of human T cells was followed by an injection of microbubbles coupled to antibodies against the T cell markers CD3, CD4 and CD8. Ultrasound signals correlated well with the numbers of kidney-infiltrating T cells that were subsequently observed through immunohistochemical staining and mRNA

expression of *CD3*, *CD4* and *CD8* in the same kidney tissues[39,40]. Preliminary results of a clinical trial in which T-cell-targeted scintigraphy was used to diagnose acute rejection of kidney transplant recipients confirmed that $CD3^+$ T cells are a potentially useful imaging target[41]. This approach used ^{99m}Tc conjugated to OKT3, which is an inhibitory anti-CD3 monoclonal antibody that is often used to induce immunosuppression in transplant recipients. The study included 22 transplant recipients and 22 healthy controls, and ^{99m}Tc-OKT3 kidney uptake was only increased in three transplant recipients who had biopsy-confirmed acute allograft rejection. Larger clinical studies are needed to assess the detection limits and the best time frames for imaging with this approach, which would be of particular interest if it could detect early rejection with high specificity. Importantly, the OKT3 antibody is already in clinical use, which might facilitate clinical translation.

^{68}Ga-pentixafor, which is a specific ligand for CXC-chemokine receptor 4 (CXCR4), enabled the detection of leukocytes in kidney allografts using PET–MRI[42]. Among 13 kidney transplant recipients with complicated urinary tract infections, imaging identified nine patients with acute allograft infection, which was confirmed by subsequent histopathologic evaluation[42].

Scintigraphy of adoptively transferred labeled autologous cells such as leukocytes or platelets[57], was an approach developed in animal studies that was followed by initial proof-of-concept studies in patients but does not seem to have been evaluated further. For example, 100 kidney transplant patients were studied by allograft scintigraphy and Doppler ultrasound at different time points after the intravenous administration of autologous ^{99m}Tc-labeled mononuclear leukocytes[58]. Abnormal scintigraphy images detected acute rejection episodes up to three days before clinical manifestations. The positive predictive value was 100%, with negative predictive values of 95% and 99% for rejection and acute tubular necrosis, respectively. However, labeling autologous cells is a complex and costly process, which might have hindered further development of this approach.

Overall, the above studies (Table 2) suggest that molecular imaging might allow non-invasive and early detection of transplant rejection and thereby facilitate timely treatment and improvement of long-term outcomes[58].

Diabetic kidney disease

Diabetic kidney disease affects ~20–25% of patients with type 2 diabetes mellitus (T2DM). Active sodium–glucose cotransporters (SGLTs) expressed at the apical side of tubular cells mediate tubular reabsorption of glucose from the urine, whereas facilitative GLUT uniporters at the basolateral cell membrane transport glucose from the tubular cells back into the bloodstream[59]. SGLT2 is responsible for the reabsorption of >90% of filtered glucose and its expression is upregulated in patients with T2DM. SGLT2 inhibitors markedly improve cardiovascular and kidney outcomes in patients with heart and/or kidney disease, with and without diabetes[60,61]. Imaging of SGLT2 *via* dynamic ^{18}F-FDG-PET–MRI was used in 20 patients with T2DM and 24 healthy volunteers to assess their responses of treatment with SGLT2 inhibitors — empagliflozin or dapagliflozin[62]. Mean transit time **[G]** was higher in patients with diabetes compared with healthy individuals, but was significantly

reduced following SGLT2 inhibition. Furthermore, kidney function determined by renal tracer uptake in the first minutes after tracer injection, was low in patients with T2DM but normalized after treatment. The authors interpreted these findings as direct *in vivo* imaging of SGLT2 transporter function because FDG is transported *via* SGLT2, albeit to a minor extent[62]. However, ^{18}F-FDG is not an appropriate tracer for examining SGLT activity because GLUT transport is responsible for 90% of ^{18}F-FDG uptake, as demonstrated in an experimental study using PET imaging in mice with genetic deletion of *Sgtl1, Sgtl2* or *Glut2* [63]. Urinary excretion of another tracer, α-methyl-4-fluoro-4-deoxy-D-glucopyranoside (Me-4 ^{18}F-FDG) was higher in *Sglt1*- and *Sgtl2*-knockout mice compared with GLUT2-deficient mice, suggesting that this tracer might be a more specific indicator of SGLT activity than ^{18}F-FDG (REF.[63]).

Another tracer — ^{11}C-methyl-D-glucoside (^{11}C-MDG) — was tested in rats as an SGLT-specific substrate. Rats with and without treatment with the SGLT2 inhibitor ipragliflozin were examined using dynamic PET. In vehicle-treated rats, intravenously injected ^{11}C-MDG accumulated substantially in the kidney cortex, whereas uptake was significantly lower in the ipragliflozin-treated animals. This decrease was dose-dependent and suggests that ipragliflozin inhibited the kidney reabsorption of ^{11}C-MDG[64]. Given the clinical efficacy and potential of SGLT2 inhibitors, tracers that enable specific SGLT2 imaging might improve our understanding of the renoprotective mechanisms of these drugs, facilitate monitoring of transporter activity and thereby drug efficacy, and guide the development of novel SGLT2 inhibitors.

Diabetes-dependent tubular injury and cell death were monitored in streptozotocin-treated rats using MRI and [1,4-$^{13}C_2$]fumarate. Diabetic rats had significant alterations in [1,4-$^{13}C_2$]fumarate uptake in the kidneys, but negligible or absent kidney-specific conversion to malate, which suggests that apoptosis, rather than necrosis, was the main cause of diabetes-induced cell death in these mice[65].

The presence of mesangial (nodular) expansion and glomerulosclerosis is characteristic of diabetic kidneys. ^{68}Ga-IRDye800-tilmanocept, which is a fluorophore-modified version of the radiopharmaceuticals ^{99m}Tc-tilmanocept and ^{68}Ga-tilmanocept (both used clinically for sentinel lymph node mapping in cancer), binds to the mannose receptor (CD206) expressed on mesangial cells. A preclinical study tested the use of ^{68}Ga-IRDye800-tilmanocept to monitor diabetes-associated changes in mesangial cells[66]. In healthy rats, glomerular uptake of the probe could be reduced in a competition experiment using a co-injected unlabeled probe, which confirmed target specificity. Histological examination further demonstrated the colocalization of CD206 and ^{68}Ga-IRDye800-tilmanocept in the glomerulus. In diabetic *db/db* mice, the probe displayed a multiphasic renal time–activity curve **[G]** that peaked at two minutes, whereas in non-diabetic *db/m* mice the peak occurred 18 min after injection. In the diabetic mice, ^{68}Ga-IRDye800-tilmanocept accumulation was faster at later stages of the disease, demonstrating its ability to monitor disease progression. However, CD206 is also expressed on cells of the monocyte lineage and whether this approach truly reflects mesangial expansion remains unclear. Nevertheless, such molecular imaging approaches have potential application in the staging of patients with diabetic kidney disease[66].

Chronic kidney disease and fibrosis

Chronic kidney disease (CKD) is associated with substantial global morbidity and mortality, and is an important risk factor for cardiovascular diseases[67,68]. Hypertension is a common feature of CKD and most patients are treated with angiotensin-converting enzyme (ACE) inhibitors or angiotensin receptor blockers[69]. Radiolabelled ^{18}F-2-fluoro-3-pent-4-yn-1-yloxypyridine (FPyKYNE)–losartan was administered to rats after 5/6 nephrectomy and PET analysis showed a reduction in the expression of renal type 1 angiotensin receptor (AT1R) 8–10 weeks after nephrectomy, which was confirmed by Western blot[70]. Treatment with the ACE inhibitor enalapril, but not the calcium channel blocker diltiazem, ameliorated progression of CKD and ^{18}F-FPyKYNE-losartan PET could detect the different *in vivo* effects of these pharmacotherapies[71].

The most consistent predictor of CKD progression is the extent of kidney fibrosis and molecular imaging might enable a non-invasive diagnostic of fibrogenesis that facilitates CKD staging and prognosis. Different probes and imaging modalities have been used to image fibrosis in liver, lung and heart disease, both in preclinical and in clinical settings[72]. For example, imaging of integrins with SPECT can capture murine myocardial infarction[73], and pulmonary fibrosis can be imaged in patients using PET[74]. Furthermore, we tested a small peptide-based elastin-specific magnetic resonance contrast agent (ESMA[75,76]) for the detection of kidney fibrosis[77]; elastin is a component of the extracellular matrix. Several *in vivo* and *ex vivo* experiments confirmed the specificity of ESMA-based molecular MRI, including comparison of signals to a non-specific contrast agent (Gd-DTPA), analysis of the amount of the molecular probe in tissues using different methods and correlation with elastin expression, as well as *ex vivo* binding and competition experiments using healthy and diseased human kidney samples[77]. The applicability of ESMA-MRI was assessed in mouse models of kidney fibrosis and at different disease stages. ESMA-MRI enabled repetitive longitudinal monitoring and staging of fibrosis development in the same animal and non-invasive monitoring of the efficacy of two different anti-fibrotic therapies[77]. Importantly, in a model of reversible kidney injury, elastin imaging detected persistent fibrosis, despite an improvement in GFR[77].

In an alternative approach, non-invasive imaging of collagen was performed in mouse models of kidney fibrosis using the collagen-binding adhesion protein (CNA35), which binds with high affinity to collagen type I and III[78]. CNA35 had previously been used to visualize collagen deposition in atherosclerotic plaques after *ex vivo* and *in vivo* administration[79]. Imaging of CNA35 enabled detection of kidney fibrosis and also revealed perivascular fibrosis, which is a common finding in both animal models and patients with CKD[80].

Collectively, these studies show that molecular imaging of kidney fibrosis is feasible and enables longitudinal fibrosis staging, monitoring of responses to anti-fibrotic treatments such as tyrosine-kinase inhibitors, and provides information on kidney pathology that extends beyond that provided by the techniques and readouts currently used (Figure 3, Table 2). Consequently, such methods might not only facilitate clinical trials and assist in the

translation of novel anti-fibrotic drugs, but might help to improve day-to-day treatment decisions and patient management in CKD[81].

Renal cell carcinoma

Molecular imaging in RCC (Table 2) is more advanced compared with that currently used in non-malignant kidney diseases, although the renal elimination of most imaging agents often limits the use of some probes in patients with kidney cancer compared with those with other malignancies. ^{18}F-FDG is the standard radiopharmaceutical used for tumour imaging and can be used to stage tumours[82], predict treatment response[83–86] and evaluate responses to treatment[87,88] in clear cell RCC (ccRCC). However, in a cohort of patients with metastatic RCC, ^{18}F-FDG-PET metrics correlated only moderately with tumour burden or survival after treatment with the mechanistic target of rapamycin (mTOR) inhibitor everolimus[89]. This poor correlation might have resulted from the heterogeneity in RCC subtypes within the study cohort and suggests that ^{18}F-FDG-PET imaging might only be suitable for RCC subtypes such as papillary RCC, which have high glucose uptake[89].

Tumour antigens

Several radiolabeled ligands of prostate-specific membrane antigen (PSMA; also known as glutamate carboxypeptidase II) have been introduced for molecular imaging and targeted therapy in prostate cancer[90–92]. PSMA is a membrane bound glycoprotein with C-terminal glutamate carboxypeptidase II and folate hydrolase I activity, and has a role in the maintenance of cellular homeostasis, cell migration, angiogenesis and endothelial repair[93,94]. This surface antigen is expressed on tumour cells and on the tumour vasculature, and has been detected in tumours other than prostate cancer[95], including RCC[96]. In a case report and in a small case series with five patients with metastatic ccRCC, the PSMA ligand ^{18}F-DCFPyL was taken up in primary tumours and metastases and enabled their detection with higher sensitivity than conventional CT or non-molecular MRI[97,98]. The follow-up prospective trial (NCT02687139) showed that hybrid ^{18}F-DCFPyL-PET–CT is helpful for identifying patients with oligometastatic ccRCC[99] but not appropriate for imaging other RCC subtypes[100]. In patients with ccRCC, this radiotracer might enable more accurate staging and monitoring of anti-angiogenic therapy than conventional CT. Another study of patients with RCC showed that imaging with Glu-NH-CO-NH-Lys-(Ahx)-[^{68}Ga(HBED-CC)] (^{68}Ga-PSMA) PET–CT enabled clear delineation of metastases in the primary staging of metastasic RCC[101].

One case report focused on a patient with metastatic RCC who received high-dose IL-2 and sunitinib (a tyrosine kinase inhibitor used in RCC treatment)[102]. This patient underwent imaging studies by hybrid PET–MRI after injection of ^{18}F-fluorothymidine, a radiolabeled thymidine analog that reflects cell proliferation. Two scans were performed — before the start of treatment with IL-2 and sunitinib, and 2.5 weeks after the therapy. PET images showed a strong decrease in ^{18}F-fluorothymidine uptake within the primary tumour and metastases, which demonstrates its potential to visualize reduced proliferation in cancerous tissue. Although further studies and clinical trials have been conducted to validate this pilot study and mostly confirmed the finding of positive ^{18}F-fluorothymidine uptake by

Europe PMC Funders Author Manuscripts

RCCs[103,104] (NCT01243359, NCT00499135), this approach has not yet become routine in the clinic.

Multiple other imaging methods target tumour-associated antigens in RCC. One example is CAIX, which is a membrane-bound enzyme that catalyzes the conversion of carbon dioxide to hydrogen carbonate, and is regulated by the transcription factor hypoxia-inducible factor 1α. CAIX expression is low in healthy kidneys, in oncocytomas, and in chromophobe and papillary RCCs, but is upregulated in the hypoxic environment of RCC tumours that carry *VHL* mutations[105]. Increased CAIX expression causes acidification of the tumour microenvironment, which leads to reduced cell adhesion and increased migration, thereby promoting tumour invasion and metastasis[106]. CAIX is therefore an attractive target for imaging and patient stratification. In the 1990s, the monoclonal anti-CAIX-antibody G250 was established for radioimmunotherapy and scintigraphy imaging in patients with RCC[107,108]. G250 could only be administered once owing to antibody immunogenicity and a chimeric version of G250 (cG250) was therefore developed that allowed multiple administrations. This antibody was labeled with ^{131}I for immunoscintigraphy[109–111] or with ^{124}I for immuno-PET[112,113]. In the multicenter phase III REDECT trial (NCT00606632), 195 patients underwent ^{124}I-cG250-PET before ccRCC resection. The sensitivity and specificity for disease detection were 86% and 86%, respectively, and all lesions <1cm could be visualized[112]. A 2020 study reported that nanobubbles could be functionalized with G250 nanobodies to allow molecular ultrasound imaging but *in vivo* applicability remains to be tested[114]. ^{18}F-VM4-037, which is another CAIX imaging probe for PET, also yielded promising results in a phase II pilot study in 11 patients with RCC[115] but the trial was terminated because the probe was no longer available (NCT01712685).

Small molecular agents mostly exhibit faster pharmacokinetics than antibodies, which have slower blood and non-target tissue clearance, as well as higher non-specific organ uptake. Accordingly, other CAIX detecting agents have been tested in animal studies to identify a probe superior to the cG250 antibody. Three probes showed potential in murine tumour graft models — ^{99m}Tc-(HE)3-ZCAIX:2 for SPECT[116, 111]In-XYIMSR-01 for PET[117] and ^{64}Cu-XYIMSR-06 for PET[118]. All three probes showed high tumour uptake and high tumour-to-blood and tumour-to-muscle ratios. However, these new probes have not yet been made commercially available and are therefore not available for clinical use.

Angiogenesis

The imaging of angiogenesis in RCC using the radiolabeled anti-vascular endothelial growth factor A (VEGF-A) monoclonal antibody ^{89}Zr-bevacizumabhas also been evaluated. VEGF is a major angiogenic factor and various cancers are treated with anti-angiogenic drugs. The establishment of an imaging approach for detecting VEGF-A might therefore be beneficial for patient treatment selection. Patients with RCC treated with either bevacizumab and IFN-α, or sunitinib received ^{89}Zr-bevacizumab hybrid PET-CT scans before therapy, and two and six weeks after therapy initiation (NCT00831857)[119]. Tracer uptake in tumours was high but strong inter-patient and intra-patient variability was observed. Bevacizumab–IFN-α treatment potently decreased tumour tracer uptake, whereas sunitinib only induced a modest reduction[119]. A similar reduction in ^{89}Zr-bevacizumab PET–CT signals was observed in

patients treated with everolimus (NCT01028638)[120]. Other molecular probes that target angiogenesis-relevant molecules are being tested in preclinical studies, including VEGF receptor 2 (VEGFR2)-targeted microbubbles for ultrasound imaging, which have already been clinically tested in prostate cancer [121] and have shown promising results in mice with RCC tumor grafts[122,123].

^{18}F-fluciclatide is a small synthetic peptide that binds to $\alpha_v\beta_3$ and $\alpha_v\beta_5$ integrins, which are expressed on endothelial cells and therefore represent a target for imaging tumour vasculature. Uptake of this probe was measured in patients with solid tumours using PET imaging (NCT00918281)[124]. In 11 patients with RCC, the imaging protocol was well tolerated and the tracer was detectable in all tumours of all patients. The degree of probe uptake varied according to RCC subtype and was higher, for example, in chromophobe RCC than in non-chromophobe RCC[124].

Immunotherapy

Programmed cell death 1 ligand 1 (PD-L1) is an important immunotherapy target in RCC and its imaging has been tested in mice using ^{89}Zr-atezolizumab immuno-PET[125]. In this study, resected tumour tissue from a patient with metastatic RCC was implanted orthotopically into NOD–SCID immunocompromised mice and rapidly formed renal masses that were characterized by sarcomatoid differentiation and high levels of PD-L1 expression. Those renal masses where re-transplanted into recipient NOD–SCID mice and scans showed high uptake of ^{89}Zr-atezolizumab in hybrid PET–CT. The patient from whom the tumour was collected was initially receiving high-dose IL-2 and pazopanib (a multi-tyrosine kinase inhibitor) but was then switched to nivolumab treatment, which is an anti-PD-1 antibody that inhibits its interaction with PD-L1; this treatment led to disease remission[125]. ^{89}Zr-atezolizumab imaging has already been reported as a non-invasive approach to assess and predict clinical response to PD-L1 blockade in metastatic bladder cancer, lung cancer and breast cancer[126], and might also be a useful tool in RCC.

Collectively, most molecular imaging approaches used in nephrology have been tested in patients with RCC, perhaps in part because these approaches benefit from studies carried out in other solid tumours. However, although clinical trials have reported promising results for targets like CAIX or VEGFR2, no RCC-specific imaging approach is currently established in the clinic.

Challenges, benefits and opportunities

Most novel molecular imaging techniques are being developed in the field of precision oncology[4] and, in the kidney, most clinical trials are focused on RCC imaging (Table 3). Among all the molecular probes summarized in this review (Figure 2, Table 2), only ^{18}F-FDG, ^{99m}Tc-DMSA and ^{99m}Tc-MAG3 are commercially available and used in the clinic. The broader use of these probes might be limited by the fact that some of them are not disease-specific and reflect broad biological processes, such as increased glucose metabolism in the case of ^{18}F-FDG. The costs and availability of such molecular imaging methods represent additional potential limitations. Moreover, although nuclear molecular imaging has very high sensitivity, which enables the use of very low doses of molecular

probes (micromolar to picomolar concentrations) with no or negligible pharmacological adverse-effects, radiation exposure, as well as limited availability of reagents and equipment, remain a challenge. By contrast, ultrasound-based molecular imaging would have the potential for the broadest implementation, given the availability of the method in many nephrology clinical units. However, ultrasound is restricted to imaging of intravascular targets, which likely limits its use to only a few types of kidney disease.

Refining the pharmacokinetic properties of probes for kidney imaging is difficult. The kidney is a major elimination organ and high unspecific probe uptake can limit the accuracy of the molecular information obtained. Dynamic measurements or long waiting times after probe injection are often required to ensure that any unbound probe is eliminated. These measures might be well controlled in clinical trials but complicate the implementation of these approaches in routine clinical practice. In the case of probes with long-lasting unspecific accumulation in the kidney, which is often observed with peptide-based probes, the ratio of target-bound to passively accumulated probe might improve with longer monitoring periods. However, this need for prolonged monitoring requires the use of radionuclides with a longer half-life that can be imaged several hours or even days after injection such as ^{89}Zr.

Importantly, despite the promising proof-of-concept studies for most molecular imaging approaches summarized in this article, which represent post-hoc group comparisons, clinical superiority to the established imaging approaches and to some emerging functional kidney analysis methods remains to be demonstrated. For successful clinical translation, new diagnostic methods must be shown to provide higher diagnostic confidence than the diagnostic methods that are already used routinely. Alternatively, the same accuracy should be reached at lower cost, lower risk and/or higher patient comfort.

Novel methods for non-invasive analysis of kidney function include renal ultrasound elastography to analyze parenchymal stiffness, and thereby kidney damage and fibrosis, ^{68}Ga-EDTA-PET imaging to analyze kidney perfusion and GFR, or intravoxel incoherent motion diffusion-weighted imaging (IVIM-DWI), which is an MRI sequence that assesses tissue diffusion of water and microcapillary perfusion separately. Some studies showed good correlations between IVIM-DWI parameters and kidney fibrosis[127] or kidney transplant rejection[128]. However, these approaches detect tissue changes that indirectly reflect functional, or morphological and/or mechanical properties of the diseased kidney, rather than changes in a specific molecule or pathway. By contrast, molecular imaging enables direct visualization of a specific molecular target, which makes it more specific and thereby less prone to misinterpretation.

Furthermore, current advances in the generation and analysis of big data, often obtained within large consortia, should enable improvements in precision medicine in nephrology through the collection and integration of large collections of clinical, pathological and molecular data from patients with kidney disease, and might lead to the identification of novel relevant targets that are suitable for specific non-invasive molecular imaging[129]. Methodological examples of such omics approaches applied to kidney research include gene expression profiling by RNA sequencing (RNA-seq) either from whole tissues (bulk RNA-

seq) or individual cells (single-cell RNA-Seq), and protein expression profiling through mass spectrometry techniques such as matrix-assisted laser desorption ionization-mass spectrometry imaging (MALDI-MSI). For example, a 2020 study of scRNA-seq applied to mice and patients with CKD elucidated the origin and profile of myofibroblasts in kidney fibrosis, and provided a basis for confirming known biomarkers, and identifying new potential targets for molecular imaging in kidney fibrosis[130]. MALDI-MSI of kidney biopsy samples has also identified several potential biomarkers, including molecules that can distinguish diabetic from hypertensive kidney disease, identify patients with glomerulonephritis with a high probability for disease progression, and predict treatment responses in patients with membranous nephropathy[131–134]. Successful integration of molecular MALDI-MSI and MRI data has already been performed and provides an interesting future avenue in kidney imaging research[135]. The identification of the autoantigen phospholipase A2 receptor (PLA2R) in membranous nephropathy is another example of how molecules identified *via* proteomic mass spectrometry can clarify disease pathophysiology, and improve diagnostics and treatment[136,137]. Overall, omics-based approaches are expected to be useful in identifying novel specific targets for non-invasive molecular imaging, that either reflect broader pathophysiological processes, such as fibrosis, sclerosis or inflammation, or disease- and treatment-specific molecules.

Any potential new target for molecular imaging needs to be thoroughly validated, for example through molecular, biochemical and histological methods, followed by experiments to test their sensitivity, specificity and pharmacokinetics *in vivo*. Successful translation of a molecular imaging approach also typically requires impact on clinical decision making. In cancer, for example, molecular imaging supports diagnostics in combination with other clinical diagnostic parameters. Biochemical design, handling and potential toxicity of the probes, as well as the costs of the imaging approach, are additional important factors. However, only few preclinical and clinical studies performed in kidney disease have tackled all of these issues in sufficient depth, perhaps because such studies require a broad interdisciplinary team of experts. If a molecular probe fulfills all the prerequisites, non-invasive imaging can help to refine diagnostics and be used to monitor disease activity specifically and longitudinally. These approaches can also be used to define novel clinical trial endpoints or serve as a companion diagnostic that guides patient stratification for safe and effective use of drugs, and thereby promote successful clinical translation[81] (Fig. 1).

The latest developments in the field of nanotechnology might also open up new possibilities for imaging and theranostics. Many nanoparticles, regardless of whether they are conjugated to a specific molecular binding agent, are retained in the kidney unspecifically owing to their size, shape, charge and/or surface properties[138]. Depending on these properties, nanoparticles have been shown to interact with the endothelial glycocalyx[138], glomerular basement membrane[139], glomerular mesangium[140] or kidney tubules[141]. Functionalization of nanoparticles with targeting ligands can enhance some of these interactions. For example, nanocarriers coupled with lambda light chains were shown to target megalin-expressing proximal tubule cells and RCC tumour cells[142]. However, implementation of nanoparticles for imaging is complex because their pharmacokinetics are difficult to control and unspecific uptake by other tissues or cells, such as macrophages, can occur[143].

Non-invasive imaging has several advantages compared with the conventional disease biomarkers currently used in the clinic. Standard laboratory analyses in nephrology rely mainly on GFR, urinary sediment and proteinuria, as well as serum or urine biomarkers of AKI, including urinary tissue inhibitor of metalloproteinase 2 (TIMP2), NGAL and kidney injury molecule 1 (KIM1)[144]. However, early AKI diagnosis or the diagnosis of kidney fibrosis, for example, remain challenging. Various urinary biomarkers of fibrosis have been evaluated, including transforming growth factor β1, connective tissue growth factor, collagen type IV[145], and specific collagen I and III degradation or production fragments[146,147]. However, none of these biomarkers provided sufficient kidney disease-specific information and thus none have been implemented in the clinic. In contrast to liquid urinary biomarkers, non-invasive imaging provides a direct insight into both kidneys and can depict particular sites and patterns of kidney damage. Moreover, in contrast to kidney biopsies, imaging displays the whole kidney and thereby avoids potential sampling errors. Molecular imaging is often combined with conventional anatomical (for example, CT) or functional (for example, MRI) imaging, which provides a multimodal diagnostic approach, that might further improve the depth of data for each particular patient.

Conclusion

Nephrology currently lacks non-invasive measures that reflect intrarenal disease activity specifically and at the molecular level. Molecular imaging might not only allow a direct glimpse into kidney-specific pathological processes but might also facilitate clinical trials of novel targeted therapies, which would improve patient stratification and therapy management as a companion diagnostics approach. Currently, most molecular imaging approaches have not yet been translated from preclinical models into the clinic, partly owing to the inherent difficulty of imaging pathological molecular processes in the kidneys. We are confident that specific molecular imaging of pathological processes within the kidneys could be used for disease staging and prognosis, monitoring of treatment responses, and to improve patient management if the correct target is defined. Such advance would bring us closer to precision medicine in nephrology.

Acknowledgements

This work was funded by the German Research Foundation (DFG; SFB/TRR57 P25&P33, SFB/TRR219 Project-ID 322900939, BO3755/13-1 Project-ID 454024652, Research Training Group 331065168), the German Federal Ministry of Education and Research (BMBF: STOP-FSGS-01GM1901A), the German Federal Ministry of Economic Affairs and Energy (BMWi: EMPAIA project), the Medical Faculty of the RWTH Aachen (START 109/20), the European Research Council (ERC: CoG-864121 Meta-Targeting and 101001791 AIM.imaging.CKD), the ITN INTRICARE of European Union's Horizon 2020 research and innovation program under the Marie Sklodowska Curie (grant 722609).

References

1. Thakur ML, Lentle BC. Snm & Radiological Society of North, A. Joint SNM/RSNA Molecular Imaging Summit Statement. J Nucl Med. 2005; 46 :11N–13N. 42N
2. Mankoff DA. A definition of molecular imaging. J Nucl Med. 2007; 48 18N, 21N
3. Ehlerding EB, England CG, McNeel DG, Cai W. Molecular Imaging of Immunotherapy Targets in Cancer. J Nucl Med. 2016; 57 :1487–1492. DOI: 10.2967/jnumed.116.177493 [PubMed: 27469363]

4. Mankoff DA, Farwell MD, Clark AS, Pryma DA. Making Molecular Imaging a Clinical Tool for Precision Oncology: A Review. JAMA Oncol. 2017; 3 :695–701. DOI: 10.1001/jamaoncol.2016.5084 [PubMed: 28033451]
5. Allali G, et al. Brain imaging of locomotion in neurological conditions. Neurophysiol Clin. 2018; 48 :337–359. DOI: 10.1016/j.neucli.2018.10.004 [PubMed: 30487063]
6. Chen IY, Wu JC. Cardiovascular molecular imaging: focus on clinical translation. Circulation. 2011; 123 :425–443. DOI: 10.1161/CIRCULATIONAHA.109.916338 [PubMed: 21282520]
7. Farber G, et al. The Future of Cardiac Molecular Imaging. Semin Nucl Med. 2020; 50 :367–385. DOI: 10.1053/j.semnuclmed.2020.02.005 [PubMed: 32540033]
8. Taylor AT. Radionuclides in nephrourology, part 1: Radiopharmaceuticals, quality control, and quantitative indices. JNucl Med. 2014; 55 :608–615. DOI: 10.2967/jnumed.113.133447 [PubMed: 24549283]
9. Taylor AT, Lipowska M, Cai H. 99mTc(CO)3(NTA) and 131I-OIH: comparable plasma clearances in patients with chronic kidney disease. J Nucl Med. 2013; 54 :578–584. DOI: 10.2967/jnumed.112.108357 [PubMed: 23424193]
10. Jaksic E, et al. Clinical investigations of 99mTc-p-aminohippuric acid as a new renal agent. Nucl Med Commun. 2009; 30 :76–81. DOI: 10.1097/mnm.0b013e328314b8bc [PubMed: 19306517]
11. Nguyen DL, et al. Reproducibility of differential renal function measurement using technetium-99m-ethylenedicysteine dynamic renal scintigraphy: a French prospective multicentre study. Nucl Med Commun. 2018; 39 :10–15. DOI: 10.1097/MNM.0000000000000769 [PubMed: 28984816]
12. Stoffel M, et al. Evaluation of technetium-99m-L,L-EC in renal transplant recipients: a comparative study with technetium-99m-MAG3 and iodine-125-OIH. J Nucl Med. 1994; 35 :1951–1958. [PubMed: 7989976]
13. Weyer K, et al. Renal uptake of 99mTc-dimercaptosuccinic acid is dependent on normal proximal tubule receptor-mediated endocytosis. J Nucl Med. 2013; 54 :159–165. DOI: 10.2967/jnumed.112.110528 [PubMed: 23232279]
14. Lee BH, et al. Decreased renal uptake of (99m)Tc-DMSA in patients with tubular proteinuria. Pediatr Nephrol. 2009; 24 :2211–2216. DOI: 10.1007/s00467-009-1238-2 [PubMed: 19579036]
15. Bobot M, et al. Renal SPECT/CT with 99mTc-dimercaptosuccinic acid is a non-invasive predictive marker for the development of interstitial fibrosis in a rat model of renal insufficiency. Nephrol Dial Transplant. 2020; doi: 10.1093/ndt/gfaa374
16. Fatemikia H, et al. Comparison of 99mTc-DMSA renal scintigraphy with biochemical and histopathological findings in animal models of acute kidney injury. Mol Cell Biochem. 2017; 434 :163–169. DOI: 10.1007/s11010-017-3046-5 [PubMed: 28466457]
17. Hitzel A, et al. Quantitative analysis of 99mTc-DMSA during acute pyelonephritis for prediction of long-term renal scarring. J Nucl Med. 2004; 45 :285–289. [PubMed: 14960649]
18. Stieger B, Unadkat JD, Prasad B, Langer O, Gali H. Role of (drug) transporters in imaging in health and disease. Drug Metab Dispos. 2014; 42 :2007–2015. DOI: 10.1124/dmd.114.059873 [PubMed: 25249691]
19. Santos AI, et al. Interobserver agreement on cortical tracer transit in 99mTc-MAG3 renography applied to congenital hydronephrosis. Nucl Med Commun. 2017; 38 :124–128. DOI: 10.1097/MNM.0000000000000620 [PubMed: 27851658]
20. Funahashi Y, et al. Effect of warm ischemia on renal function during partial nephrectomy: assessment with new 99mTc-mercaptoacetyltriglycine scintigraphy parameter. Urology. 2012; 79 :160–164. DOI: 10.1016/j.urology.2011.08.071 [PubMed: 22070892]
21. Pathuri G, et al. Evaluation of (99m)Tc-probestin SPECT as a novel technique for noninvasive imaging of kidney aminopeptidase N expression. Mol Pharm. 2014; 11 :2948–2953. DOI: 10.1021/mp5002872 [PubMed: 24988047]
22. Longo DL, Busato A, Lanzardo S, Antico F, Aime S. Imaging the pH evolution of an acute kidney injury model by means of iopamidol, a MRI-CEST pH-responsive contrast agent. Magn Reson Med. 2013; 70 :859–864. DOI: 10.1002/mrm.24513 [PubMed: 23059893]

23. Irrera P, Consolino L, Cutrin JC, Zollner FG, Longo DL. Dual assessment of kidney perfusion and pH by exploiting a dynamic CEST-MRI approach in an acute kidney ischemia-reperfusion injury murine model. NMR Biomed. 2020; 33 e4287 doi: 10.1002/nbm.4287 [PubMed: 32153058]
24. Clatworthy MR, et al. Magnetic resonance imaging with hyperpolarized [1,4-C-13(2)]fumarate allows detection of early renal acute tubular necrosis. PNatl Acad Sci USA. 2012; 109 :13374–13379. DOI: 10.1073/pnas.1205539109
25. Nielsen PM, et al. Fumarase activity: an in vivo and in vitro biomarker for acute kidney injury. Sci Rep. 2017; 7 40812 doi: 10.1038/srep40812 [PubMed: 28094329]
26. Gallagher FA, et al. Production of hyperpolarized [1,4-13C2]malate from [1,4-13C2]fumarate is a marker of cell necrosis and treatment response in tumors. Proc Natl Acad Sci U S A. 2009; 106 :19801–19806. DOI: 10.1073/pnas.0911447106 [PubMed: 19903889]
27. Huang J, Li J, Lyu Y, Miao Q, Pu K. Molecular optical imaging probes for early diagnosis of drug-induced acute kidney injury. Nat Mater. 2019; 18 :1133–1143. DOI: 10.1038/s41563-019-0378-4 [PubMed: 31133729]
28. Allison SJ. A molecular imaging approach for the early, real-time diagnosis of acute kidney injury. Nat Rev Nephrol. 2019; 15 :458. doi: 10.1038/s41581-019-0165-0
29. Akhtar AM, et al. In vivo quantification of VCAM-1 expression in renal ischemia reperfusion injury using non-invasive magnetic resonance molecular imaging. PLoS One. 2010; 5 e12800 doi: 10.1371/journal.pone.0012800 [PubMed: 20877722]
30. Hoyt K, et al. Molecular Ultrasound Imaging of Tissue Inflammation Using an Animal Model of Acute Kidney Injury. Mol Imaging Biol. 2015; 17 :786–792. DOI: 10.1007/s11307-015-0860-6 [PubMed: 25905474]
31. Boesen EI, Crislip GR, Sullivan JC. Use of ultrasound to assess renal reperfusion and P-selectin expression following unilateral renal ischemia. Am J Physiol Renal Physiol. 2012; 303 :F1333–1340. DOI: 10.1152/ajprenal.00406.2012 [PubMed: 22933301]
32. Andonian S, Coulthard T, Smith AD, Singhal PS, Lee BR. Real-time quantitation of renal ischemia using targeted microbubbles: in-vivo measurement of P-selectin expression. J Endourol. 2009; 23 :373–378. DOI: 10.1089/end.2008.0229 [PubMed: 19245294]
33. Atukorale PU, Covarrubias G, Bauer L, Karathanasis E. Vascular targeting of nanoparticles for molecular imaging of diseased endothelium. Adv Drug Deliv Rev. 2017; 113 :141–156. DOI: 10.1016/j.addr.2016.09.006 [PubMed: 27639317]
34. Guler R, Svedmark SF, Abouzayed A, Orlova A, Lofblom J. Increasing thermal stability and improving biodistribution of VEGFR2-binding affibody molecules by a combination of in silico and directed evolution approaches. Sci Rep. 2020; 10 18148 doi: 10.1038/s41598-020-74560-5 [PubMed: 33097752]
35. Wan CH, Tseng JR, Lee MH, Yang LY, Yen TC. Clinical utility of FDG PET/CT in acute complicated pyelonephritis-results from an observational study. Eur J Nucl Med Mol Imaging. 2018; 45 :462–470. DOI: 10.1007/s00259-017-3835-9 [PubMed: 28951990]
36. Pijl JP, Glaudemans A, Slart R, Kwee TC. (18)F-FDG PET/CT in Autosomal Dominant Polycystic Kidney Disease Patients with Suspected Cyst Infection. J Nucl Med. 2018; 59 :1734–1741. DOI: 10.2967/jnumed.117.199448 [PubMed: 29653972]
37. Tseng JR, et al. Clinical Usefulness of (1)(8)f-FDG PET/CT for the Detection of Infections of Unknown Origin in Patients Undergoing Maintenance Hemodialysis. J Nucl Med. 2015; 56 :681–687. DOI: 10.2967/jnumed.114.151696 [PubMed: 25766894]
38. George EA, Codd JE, Newton WT, Haibach H, Donati RM. Comparative evaluation of renal transplant rejection with radioiodinated fibrinogen 99mTc-sulfur collid, and 67Ga-citrate. J Nucl Med. 1976; 17 :175–180. [PubMed: 765436]
39. Grabner A, et al. Renal Contrast-Enhanced Sonography Findings in a Model of Acute Cellular Allograft Rejection. Am J Transplant. 2016; 16 :1612–1619. DOI: 10.1111/ajt.13648 [PubMed: 26613381]
40. Grabner A, et al. Noninvasive Imaging of Acute Renal Allograft Rejection by Ultrasound Detection of Microbubbles Targeted to T-lymphocytes in Rats. Ultraschall Med. 2016; 37 :82–91. DOI: 10.1055/s-0034-1385796 [PubMed: 25919412]

41. Martins FP, Souza SA, Goncalves RT, Fonseca LM, Gutfilen B. Preliminary results of [99mTc]OKT3 scintigraphy to evaluate acute rejection in renal transplants. Transplant Proc. 2004; 36 :2664–2667. DOI: 10.1016/j.transproceed.2004.09.085 [PubMed: 15621118]
42. Derlin T, et al. Integrating MRI and Chemokine Receptor CXCR4-Targeted PET for Detection of Leukocyte Infiltration in Complicated Urinary Tract Infections After Kidney Transplantation. J Nucl Med. 2017; 58 :1831–1837. DOI: 10.2967/jnumed.117.193037 [PubMed: 28450555]
43. Sargsyan SA, et al. Detection of glomerular complement C3 fragments by magnetic resonance imaging in murine lupus nephritis. Kidney Int. 2012; 81 :152–159. DOI: 10.1038/ki.2011.332 [PubMed: 21956190]
44. Serkova NJ, et al. Renal inflammation: targeted iron oxide nanoparticles for molecular MR imaging in mice. Radiology. 2010; 255 :517–526. DOI: 10.1148/radiol.09091134 [PubMed: 20332377]
45. Huang Q, et al. C5b-9-targeted molecular MR imaging in rats with Heymann nephritis: a new approach in the evaluation of nephrotic syndrome. PLoS One. 2015; 10 e0121244 doi: 10.1371/journal.pone.0121244 [PubMed: 25774523]
46. Smith RJH, et al. C3 glomerulopathy - understanding a rare complement-driven renal disease. Nat Rev Nephrol. 2019; 15 :129–143. DOI: 10.1038/s41581-018-0107-2 [PubMed: 30692664]
47. Hanssen O, et al. Non-invasive approaches in the diagnosis of acute rejection in kidney transplant recipients. Part I. In vivo imaging methods. Clin Kidney J. 2017; 10 :97–105. DOI: 10.1093/ckj/sfw062 [PubMed: 28643821]
48. Lovinfosse P, et al. Fluorodeoxyglucose F(18) Positron Emission Tomography Coupled With Computed Tomography in Suspected Acute Renal Allograft Rejection. Am J Transplant. 2016; 16 :310–316. DOI: 10.1111/ajt.13429 [PubMed: 26302136]
49. Even-Sapir E, et al. Kidney allografts and remaining contralateral donor kidneys before and after transplantation: assessment by quantitative (99m)Tc-DMSA SPECT. J Nucl Med. 2002; 43 :584–588. [PubMed: 11994518]
50. Bajen MT, et al. MAG3 renogram deconvolution in kidney transplantation: utility of the measurement of initial tracer uptake. J Nucl Med. 1997; 38 :1295–1299. [PubMed: 9255171]
51. Benjamens S, et al. Limited clinical value of two consecutive post-transplant renal scintigraphy procedures. Eur Radiol. 2020; 30 :452–460. DOI: 10.1007/s00330-019-06334-1 [PubMed: 31338652]
52. Erbas B. Peri- and Postsurgical Evaluations of Renal Transplant. Semin Nucl Med. 2017; 47 :647–659. DOI: 10.1053/j.semnuclmed.2017.07.002 [PubMed: 28969763]
53. George EA, Codd JE, Newton WT, Donati RM. 67Ga citrate in renal allograft rejection. Radiology. 1975; 117 :731–733. DOI: 10.1148/117.3.731 [PubMed: 1103231]
54. Solaric-George EA, Fletcher JW, Newton WT, Henry RE, Donati RM. Renal accumulation of 99mTc sulfur colloid in transplant rejection. Radiology. 1974; 111 :465–466. DOI: 10.1148/111.2.465 [PubMed: 4594542]
55. George EA, Codd JE, Newton WT, Henry RE, Donati RM. Further evaluation of 99m-Tc sulfur colloid accumulation in rejecting renal transplants in man and a canine model. Radiology. 1975; 116 :121–126. DOI: 10.1148/116.1.121 [PubMed: 1094488]
56. Liao T, et al. Noninvasive quantification of intrarenal allograft C4d deposition with targeted ultrasound imaging. Am J Transplant. 2019; 19 :259–268. DOI: 10.1111/ajt.15105 [PubMed: 30171802]
57. Martin-Comin J. Kidney graft rejection studies with labeled platelets and lymphocytes. Int J Rad Appl Instrum B. 1986; 13 :173–181. DOI: 10.1016/0883-2897(86)90233-3 [PubMed: 3533855]
58. Lopes de Souza SA, et al. Diagnosis of renal allograft rejection and acute tubular necrosis by 99mTc-mononuclear leukocyte imaging. Transplant Proc. 2004; 36 :2997–3001. DOI: 10.1016/j.transproceed.2004.11.100 [PubMed: 15686680]
59. Szablewski L. Distribution of glucose transporters in renal diseases. J Biomed Sci. 2017; 24 :64. doi: 10.1186/s12929-017-0371-7 [PubMed: 28854935]
60. Neuen BL, et al. SGLT2 inhibitors for the prevention of kidney failure in patients with type 2 diabetes: a systematic review and meta-analysis. Lancet Diabetes Endocrinol. 2019; 7 :845–854. DOI: 10.1016/S2213-8587(19)30256-6 [PubMed: 31495651]

61. Heerspink HJL, et al. Dapagliflozin in Patients with Chronic Kidney Disease. N Engl J Med. 2020; doi: 10.1056/NEJMoa2024816
62. Rasul S, et al. Response evaluation of SGLT2 inhibitor therapy in patients with type 2 diabetes mellitus using (18)F-FDG PET/MRI. BMJ Open Diabetes Res Care. 2020; 8 doi: 10.1136/bmjdrc-2019-001135
63. Sala-Rabanal M, et al. Revisiting the physiological roles of SGLTs and GLUTs using positron emission tomography in mice. J Physiol. 2016; 594 :4425–4438. DOI: 10.1113/JP271904 [PubMed: 27018980]
64. Mitsuoka K, et al. Functional imaging of pharmacological action of SGLT2 inhibitor ipragliflozin via PET imaging using (11)C-MDG. Pharmacol Res Perspect. 2016; 4 e00244 doi: 10.1002/prp2.244 [PubMed: 28116097]
65. Laustsen C, et al. Hyperpolarized [1,4-(13)C]fumarate imaging detects microvascular complications and hypoxia mediated cell death in diabetic nephropathy. Sci Rep. 2020; 10 9650 doi: 10.1038/s41598-020-66265-6 [PubMed: 32541797]
66. Qin Z, et al. Molecular Imaging of the Glomerulus via Mesangial Cell Uptake of Radiolabeled Tilmanocept. J Nucl Med. 2019; 60 :1325–1332. DOI: 10.2967/jnumed.118.223727 [PubMed: 30796169]
67. Webster AC, Nagler EV, Morton RL, Masson P. Chronic Kidney Disease. Lancet. 2017; 389 :1238–1252. DOI: 10.1016/S0140-6736(16)32064-5 [PubMed: 27887750]
68. Collaboration, G. B. D. C. K. D. Global, regional, and national burden of chronic kidney disease, 1990-2017: a systematic analysis for the Global Burden of Disease Study 2017. Lancet. 2020; 395 :709–733. DOI: 10.1016/S0140-6736(20)30045-3 [PubMed: 32061315]
69. Ku E, Lee BJ, Wei J, Weir MR. Hypertension in CKD: Core Curriculum 2019. Am J Kidney Dis. 2019; 74 :120–131. DOI: 10.1053/j.ajkd.2018.12.044 [PubMed: 30898362]
70. Ismail B, et al. Decreased renal AT1 receptor binding in rats after subtotal nephrectomy: PET study with [(18)F]FPyKYNE-losartan. EJNMMI Res. 2016; 6 :55. doi: 10.1186/s13550-016-0209-4 [PubMed: 27339045]
71. Ismail B, et al. Treatment with enalapril and not diltiazem ameliorated progression of chronic kidney disease in rats, and normalized renal AT1 receptor expression as measured with PET imaging. PLoS One. 2017; 12 e0177451 doi: 10.1371/journal.pone.0177451 [PubMed: 28542215]
72. Baues M, et al. Fibrosis imaging: Current concepts and future directions. Adv Drug Deliv Rev. 2017; 121 :9–26. DOI: 10.1016/j.addr.2017.10.013 [PubMed: 29108860]
73. van den Borne SW, et al. Molecular imaging of interstitial alterations in remodeling myocardium after myocardial infarction. JAm Coll Cardiol. 2008; 52 :2017–2028. DOI: 10.1016/j.jacc.2008.07.067 [PubMed: 19055994]
74. Chen DL, Schiebler ML, Goo JM, van Beek EJR. PET imaging approaches for inflammatory lung diseases: Current concepts and future directions. Eur J Radiol. 2017; 86 :371–376. DOI: 10.1016/j.ejrad.2016.09.014 [PubMed: 27663638]
75. Makowski MR, et al. Assessment of atherosclerotic plaque burden with an elastin-specific magnetic resonance contrast agent. Nat Med. 2011; 17 :383–388. DOI: 10.1038/nm.2310 [PubMed: 21336283]
76. Ehling J, et al. Elastin-based molecular MRI of liver fibrosis. Hepatology. 2013; 58 :1517–1518. DOI: 10.1002/hep.26326 [PubMed: 23424008]
77. Sun Q, et al. Elastin imaging enables noninvasive staging and treatment monitoring of kidney fibrosis. Sci Transl Med. 2019; 11 doi: 10.1126/scitranslmed.aat4865
78. Sanders HM, et al. The binding of CNA35 contrast agents to collagen fibrils. Chem Commun (Camb). 2011; 47 :1503–1505. DOI: 10.1039/c0cc02901g [PubMed: 21088778]
79. Megens RT, et al. Imaging collagen in intact viable healthy and atherosclerotic arteries using fluorescently labeled CNA35 and two-photon laser scanning microscopy. Mol Imaging. 2007; 6 :247–260. [PubMed: 17711780]
80. Baues M, et al. A collagen-binding protein enables molecular imaging of kidney fibrosis in vivo. Kidney Int. 2020; 97 :609–614. DOI: 10.1016/j.kint.2019.08.029 [PubMed: 31784048]

81. Klinkhammer BM, Goldschmeding R, Floege J, Boor P. Treatment of Renal Fibrosis-Turning Challenges into Opportunities. Adv Chronic Kidney Dis. 2017; 24 :117–129. DOI: 10.1053/j.ackd.2016.11.002 [PubMed: 28284377]
82. Ak I, Can C. F-18 FDG PET in detecting renal cell carcinoma. Acta Radiol. 2005; 46 :895–899. DOI: 10.1080/02841850500335002 [PubMed: 16392617]
83. Khandani AH, Cowey CL, Moore DT, Gohil H, Rathmell WK. Primary renal cell carcinoma: relationship between 18F-FDG uptake and response to neoadjuvant sorafenib. Nucl Med Commun. 2012; 33 :967–973. DOI: 10.1097/MNM.0b013e3283561837 [PubMed: 22714005]
84. Tabei T, et al. Early assessment with (18)F-2-fluoro-2-deoxyglucose positron emission tomography/computed tomography to predict short-term outcome in clear cell renal carcinoma treated with nivolumab. BMC Cancer. 2019; 19 :298. doi: 10.1186/s12885-019-5510-y [PubMed: 30940117]
85. Nakaigawa N, et al. FDG PET/CT as a prognostic biomarker in the era of molecular-targeting therapies: max SUVmax predicts survival of patients with advanced renal cell carcinoma. BMC Cancer. 2016; 16 :67. doi: 10.1186/s12885-016-2097-4 [PubMed: 26857818]
86. Minamimoto R, Barkhodari A, Harshman L, Srinivas S, Quon A. Prognostic Value of Quantitative Metabolic Metrics on Baseline Pre-Sunitinib FDG PET/CT in Advanced Renal Cell Carcinoma. PLoS One. 2016; 11 e0153321 doi: 10.1371/journal.pone.0153321 [PubMed: 27123976]
87. Vercellino L, et al. 18F-FDG PET/CT imaging for an early assessment of response to sunitinib in metastatic renal carcinoma: preliminary study. Cancer Biother Radiopharm. 2009; 24 :137–144. DOI: 10.1089/cbr.2008.0527 [PubMed: 19243256]
88. Kelly-Morland C, et al. Evaluation of treatment response and resistance in metastatic renal cell cancer (mRCC) using integrated (18)F-Fluorodeoxyglucose ((18)F-FDG) positron emission tomography/magnetic resonance imaging (PET/MRI); The REMAP study. BMC Cancer. 2017; 17 :392. doi: 10.1186/s12885-017-3371-9 [PubMed: 28578690]
89. Chen JL, et al. FDG-PET as a predictive biomarker for therapy with everolimus in metastatic renal cell cancer. Cancer Med. 2013; 2 :545–552. DOI: 10.1002/cam4.102 [PubMed: 24156027]
90. Fendler WP, et al. (68)Ga-PSMA PET/CT: Joint EANM and SNMMI procedure guideline for prostate cancer imaging: version 1.0. Eur J Nucl Med Mol Imaging. 2017; 44 :1014–1024. DOI: 10.1007/s00259-017-3670-z [PubMed: 28283702]
91. Kratochwil C, et al. EANM procedure guidelines for radionuclide therapy with (177)Lu-labelled PSMA-ligands ((177)Lu-PSMA-RLT). Eur J Nucl Med Mol Imaging. 2019; 46 :2536–2544. DOI: 10.1007/s00259-019-04485-3 [PubMed: 31440799]
92. Beheshti M, et al. Multiphasic (68)Ga-PSMA PET/CT in the Detection of Early Recurrence in Prostate Cancer Patients with a PSA Level of Less Than 1 ng/mL: A Prospective Study of 135 Patients. J Nucl Med. 2020; 61 :1484–1490. DOI: 10.2967/jnumed.119.238071 [PubMed: 32060214]
93. Endepols H, et al. In vivo Molecular Imaging of Glutamate Carboxypeptidase II Expression in Re-endothelialisation after Percutaneous Balloon Denudation in a Rat Model. Sci Rep. 2018; 8 7411 doi: 10.1038/s41598-018-25863-1 [PubMed: 29743623]
94. Whitaker HC, et al. N-acetyl-L-aspartyl-L-glutamate peptidase-like 2 is overexpressed in cancer and promotes a pro-migratory and pro-metastatic phenotype. Oncogene. 2014; 33 :5274–5287. DOI: 10.1038/onc.2013.464 [PubMed: 24240687]
95. Morgenroth A, et al. Targeting of prostate-specific membrane antigen for radio-ligand therapy of triple-negative breast cancer. Breast Cancer Res. 2019; 21 :116. doi: 10.1186/s13058-019-1205-1 [PubMed: 31640747]
96. Siva S, et al. Expanding the role of small-molecule PSMA ligands beyond PET staging of prostate cancer. Nat Rev Urol. 2020; 17 :107–118. DOI: 10.1038/s41585-019-0272-5 [PubMed: 31937920]
97. Rowe SP, et al. Imaging of metastatic clear cell renal cell carcinoma with PSMA-targeted (1)(8)F-DCFPyL PET/CT. Ann Nucl Med. 2015; 29 :877–882. DOI: 10.1007/s12149-015-1017-z [PubMed: 26286635]
98. Chen Y, et al. 2-(3-{1-Carboxy-5-[(6-[18F]fluoro-pyridine-3-carbonyl)-amino]-pentyl}-ureido)-pen tanedioic acid, [18F]DCFPyL, a PSMA-based PET imaging agent for prostate cancer. Clin Cancer Res. 2011; 17 :7645–7653. DOI: 10.1158/1078-0432.CCR-11-1357 [PubMed: 22042970]

99. Meyer AR, et al. Improved identification of patients with oligometastatic clear cell renal cell carcinoma with PSMA-targeted (18)F-DCFPyL PET/CT. Ann Nucl Med. 2019; 33 :617–623. DOI: 10.1007/s12149-019-01371-8 [PubMed: 31147927]

100. Yin Y, et al. Inconsistent Detection of Sites of Metastatic Non-Clear Cell Renal Cell Carcinoma with PSMA-Targeted [(18)F]DCFPyL PET/CT. Mol Imaging Biol. 2019; 21 :567–573. DOI: 10.1007/s11307-018-1271-2 [PubMed: 30218388]

101. Sawicki LM, et al. Diagnostic potential of PET/CT using a (68)Ga-labelled prostate-specific membrane antigen ligand in whole-body staging of renal cell carcinoma: initial experience. Eur J Nucl Med Mol Imaging. 2017; 44 :102–107. DOI: 10.1007/s00259-016-3360-2 [PubMed: 26996777]

102. Valls L, et al. Early response monitoring of receptor tyrosine kinase inhibitor therapy in metastatic renal cell carcinoma using [F-18]fluorothymidine-positron emission tomography-magnetic resonance. Semin Roentgenol. 2014; 49 :238–241. DOI: 10.1053/j.ro.2014.09.001 [PubMed: 25497908]

103. Ukon N, et al. Dynamic PET evaluation of elevated FLT level after sorafenib treatment in mice bearing human renal cell carcinoma xenograft. EJNMMI Res. 2016; 6 :90. doi: 10.1186/s13550-016-0246-z [PubMed: 27957722]

104. Wong PK, et al. In vivo imaging of cellular proliferation in renal cell carcinoma using 18F-fluorothymidine PET. Asia Ocean J Nucl Med Biol. 2014; 2 :3–11. [PubMed: 27408853]

105. Stillebroer AB, Mulders PF, Boerman OC, Oyen WJ, Oosterwijk E. Carbonic anhydrase IX in renal cell carcinoma: implications for prognosis, diagnosis, and therapy. Eur Urol. 2010; 58 :75–83. DOI: 10.1016/j.eururo.2010.03.015 [PubMed: 20359812]

106. Pastorek J, Pastorekova S. Hypoxia-induced carbonic anhydrase IX as a target for cancer therapy:from biology to clinical use. Semin Cancer Biol. 2015; 31 :52–64. DOI: 10.1016/j.semcancer.2014.08.002 [PubMed: 25117006]

107. Oosterwijk E, et al. Antibody localization in human renal cell carcinoma: a phase I study of monoclonal antibody G250. J Clin Oncol. 1993; 11 :738–750. DOI: 10.1200/JCO.1993.11.4.738 [PubMed: 8478666]

108. Divgi CR, et al. Phase I/II radioimmunotherapy trial with iodine-131-labeled monoclonal antibody G250 in metastatic renal cell carcinoma. Clin Cancer Res. 1998; 4 :2729–2739. [PubMed: 9829736]

109. Brouwers AH, et al. 131 I-cG250 monoclonal antibody immunoscintigraphy versus [18 F]FDG-PET imaging in patients with metastatic renal cell carcinoma: a comparative study. Nucl Med Commun. 2002; 23 :229–236. DOI: 10.1097/00006231-200203000-00005 [PubMed: 11891480]

110. Brouwers AH, et al. Targeting of metastatic renal cell carcinoma with the chimeric monoclonal antibody G250 labeled with (131)I or (111)In: an intrapatient comparison. Clin Cancer Res. 2003; 9 :3953S–3960S. [PubMed: 14506194]

111. Steffens MG, et al. Targeting of renal cell carcinoma with iodine-131-labeled chimeric monoclonal antibody G250. J Clin Oncol. 1997; 15 :1529–1537. DOI: 10.1200/JCO.1997.15.4.1529 [PubMed: 9193349]

112. Divgi CR, et al. Positron emission tomography/computed tomography identification of clear cell renal cell carcinoma: results from the REDECT trial. J Clin Oncol. 2013; 31 :187–194. DOI: 10.1200/JCO.2011.41.2445 [PubMed: 23213092]

113. Pryma DA, et al. Correlation of in vivo and in vitro measures of carbonic anhydrase IX antigen expression in renal masses using antibody 124I-cG250. J Nucl Med. 2011; 52 :535–540. DOI: 10.2967/jnumed.110.083295 [PubMed: 21421715]

114. Yu Z, et al. Anti-G250 nanobody-functionalized nanobubbles targeting renal cell carcinoma cells for ultrasound molecular imaging. Nanotechnology. 2020; 31 205101 doi: 10.1088/1361-6528/ab7040 [PubMed: 32107342]

115. Turkbey B, et al. PET/CT imaging of renal cell carcinoma with (18)F-VM4-037: a phase II pilot study. Abdom Radiol (NY). 2016; 41 :109–118. DOI: 10.1007/s00261-015-0599-1 [PubMed: 26830617]

Europe PMC Funders Author Manuscripts

116. Garousi J, et al. Comparative Evaluation of Affibody Molecules for Radionuclide Imaging of in Vivo Expression of Carbonic Anhydrase IX. Mol Pharm. 2016; 13 :3676–3687. DOI: 10.1021/acs.molpharmaceut.6b00502 [PubMed: 27529191]
117. Yang X, et al. Imaging of carbonic anhydrase IX with an 111In-labeled dual-motif inhibitor. Oncotarget. 2015; 6 :33733–33742. DOI: 10.18632/oncotarget.5254 [PubMed: 26418876]
118. Minn I, et al. [64Cu]XYIMSR-06: A dual-motif CAIX ligand for PET imaging of clear cell renal cell carcinoma. Oncotarget. 2016; 7 :56471–56479. DOI: 10.18632/oncotarget.10602 [PubMed: 27437764]
119. Oosting SF, et al. 89Zr-bevacizumab PET visualizes heterogeneous tracer accumulation in tumor lesions of renal cell carcinoma patients and differential effects of antiangiogenic treatment. J Nucl Med. 2015; 56 :63–69. DOI: 10.2967/jnumed.114.144840 [PubMed: 25476536]
120. van Es SC, et al. (89)Zr-Bevacizumab PET: Potential Early Indicator of Everolimus Efficacy in Patients with Metastatic Renal Cell Carcinoma. J Nucl Med. 2017; 58 :905–910. DOI: 10.2967/jnumed.116.183475 [PubMed: 28082434]
121. Smeenge M, et al. First-in-Human Ultrasound Molecular Imaging With a VEGFR2-Specific Ultrasound Molecular Contrast Agent (BR55) in Prostate Cancer: A Safety and Feasibility Pilot Study. Invest Radiol. 2017; 52 :419–427. DOI: 10.1097/RLI.0000000000000362 [PubMed: 28257340]
122. Rojas JD, et al. Ultrasound Molecular Imaging of VEGFR-2 in Clear-Cell Renal Cell Carcinoma Tracks Disease Response to Antiangiogenic and Notch-Inhibition Therapy. Theranostics. 2018; 8 :141–155. DOI: 10.7150/thno.19658 [PubMed: 29290798]
123. Wei S, et al. Targeted contrast-enhanced ultrasound imaging of angiogenesis in an orthotopic mouse tumor model of renal carcinoma. Ultrasound Med Biol. 2014; 40 :1250–1259. DOI: 10.1016/j.ultrasmedbio.2013.12.001 [PubMed: 24613557]
124. Mena E, et al. [(1)(8)F]fluciclatide in the in vivo evaluation of human melanoma and renal tumors expressing alphavbeta 3 and alpha vbeta 5 integrins. Eur J Nucl Med Mol Imaging. 2014; 41 :1879–1888. DOI: 10.1007/s00259-014-2791-x [PubMed: 24973039]
125. Vento J, et al. PD-L1 detection using (89)Zr-atezolizumab immuno-PET in renal cell carcinoma tumorgrafts from a patient with favorable nivolumab response. J Immunother Cancer. 2019; 7 :144. doi: 10.1186/s40425-019-0607-z [PubMed: 31155004]
126. Bensch F, et al. (89)Zr-atezolizumab imaging as a non-invasive approach to assess clinical response to PD-L1 blockade in cancer. Nat Med. 2018; 24 :1852–1858. DOI: 10.1038/s41591-018-0255-8 [PubMed: 30478423]
127. Mao W, et al. Intravoxel incoherent motion diffusion-weighted imaging for the assessment of renal fibrosis of chronic kidney disease: A preliminary study. Magn Reson Imaging. 2018; 47 :118–124. DOI: 10.1016/j.mri.2017.12.010 [PubMed: 29217491]
128. Poynton CB, et al. Intravoxel incoherent motion analysis of renal allograft diffusion with clinical and histopathological correlation in pediatric kidney transplant patients: A preliminary cross-sectional observational study. Pediatr Transplant. 2017; 21 doi: 10.1111/petr.12996
129. Ong E, et al. Modelling kidney disease using ontology: insights from the Kidney Precision Medicine Project. Nat Rev Nephrol. 2020; doi: 10.1038/s41581-020-00335-w
130. Kuppe C, et al. Decoding myofibroblast origins in human kidney fibrosis. Nature. 2020; doi: 10.1038/s41586-020-2941-1
131. Smith A, et al. Detecting Proteomic Indicators to Distinguish Diabetic Nephropathy from Hypertensive Nephrosclerosis by Integrating Matrix-Assisted Laser Desorption/Ionization Mass Spectrometry Imaging with High-Mass Accuracy Mass Spectrometry. Kidney Blood Press Res. 2020; 45 :233–248. DOI: 10.1159/000505187 [PubMed: 32062660]
132. Ivanova M, et al. Matrix-assisted laser desorption/ionization mass spectrometry imaging to uncover protein alterations associated with the progression of IgA nephropathy. Virchows Arch. 2020; 476 :903–914. DOI: 10.1007/s00428-019-02705-7 [PubMed: 31838587]
133. Smith A, et al. High Spatial Resolution MALDI-MS Imaging in the Study of Membranous Nephropathy. Proteomics Clin Appl. 2019; 13 e1800016 doi: 10.1002/prca.201800016 [PubMed: 30548219]

134. Smith A, et al. alpha-1-Antitrypsin detected by MALDI imaging in the study of glomerulonephritis: Its relevance in chronic kidney disease progression. Proteomics. 2016; 16 :1759–1766. DOI: 10.1002/pmic.201500411 [PubMed: 26749278]
135. Abdelmoula WM, et al. Automatic 3D Nonlinear Registration of Mass Spectrometry Imaging and Magnetic Resonance Imaging Data. Anal Chem. 2019; 91 :6206–6216. DOI: 10.1021/acs.analchem.9b00854 [PubMed: 30932478]
136. Beck LH Jr, et al. M-type phospholipase A2 receptor as target antigen in idiopathic membranous nephropathy. N Engl J Med. 2009; 361 :11–21. DOI: 10.1056/NEJMoa0810457 [PubMed: 19571279]
137. Rinschen MM, Saez-Rodriguez J. The tissue proteome in the multi-omic landscape of kidney disease. Nat Rev Nephrol. 2020; doi: 10.1038/s41581-020-00348-5
138. Du B, Yu M, Zheng J. Transport and interactions of nanoparticles in the kidneys. Nature Reviews Materials. 2018; 3 :358–374. DOI: 10.1038/s41578-018-0038-3
139. Bennett KM, et al. Use of Cationized Ferritin Nanoparticles to Measure Renal Glomerular Microstructure with MRI. Methods Mol Biol. 2016; 1397 :67–79. DOI: 10.1007/978-1-4939-3353-2_7 [PubMed: 26676128]
140. Choi CH, Zuckerman JE, Webster P, Davis ME. Targeting kidney mesangium by nanoparticles of defined size. Proc Natl Acad Sci U S A. 2011; 108 :6656–6661. DOI: 10.1073/pnas.1103573108 [PubMed: 21464325]
141. Williams RM, et al. Selective Nanoparticle Targeting of the Renal Tubules. Hypertension. 2018; 71 :87–94. DOI: 10.1161/HYPERTENSIONAHA.117.09843 [PubMed: 29133360]
142. Ordikhani F, et al. Selective Trafficking of Light Chain-Conjugated Nanoparticles to the Kidney and Renal Cell Carcinoma. Nano Today. 2020; 35 doi: 10.1016/j.nantod.2020.100990
143. Kiessling F, Mertens ME, Grimm J, Lammers T. Nanoparticles for imaging: top or flop? Radiology. 2014; 273 :10–28. DOI: 10.1148/radiol.14131520 [PubMed: 25247562]
144. Ronco C, Bellomo R, Kellum JA. Acute kidney injury. Lancet. 2019; 394 :1949–1964. DOI: 10.1016/S0140-6736(19)32563-2 [PubMed: 31777389]
145. Tesch GH. Review: Serum and urine biomarkers of kidney disease: A pathophysiological perspective. Nephrology (Carlton). 2010; 15 :609–616. DOI: 10.1111/j.1440-1797.2010.01361.x [PubMed: 20883281]
146. Papasotiriou M, et al. Serum and urine markers of collagen degradation reflect renal fibrosis in experimental kidney diseases. Nephrol Dial Transplant. 2015; 30 :1112–1121. DOI: 10.1093/ndt/gfv063 [PubMed: 25784725]
147. Genovese F, et al. Turnover of type III collagen reflects disease severity and is associated with progression and microinflammation in patients with IgA nephropathy. Nephrol Dial Transplant. 2016; 31 :472–479. DOI: 10.1093/ndt/gfv301 [PubMed: 26311218]
148. Park UJ, et al. Use of early postoperative MAG3 renal scan to predict long-term outcomes of renal transplants. Exp Clin Transplant. 2013; 11 :118–121. DOI: 10.6002/ect.2012.0090 [PubMed: 23477352]
149. Pijl JP, Kwee TC, Slart R, Glaudemans A. FDG-PET/CT for diagnosis of cyst infection in autosomal dominant polycystic kidney disease. Clin Transl Imaging. 2018; 6 :61–67. DOI: 10.1007/s40336-017-0261-8 [PubMed: 29568734]
150. Salaman JR, Blandy JP. The use of radioactive fibrinogen as a means for detecting rejection of human renal transplants. Br J Surg. 1970; 57 :855.
151. Reuter S, et al. Potential of noninvasive serial assessment of acute renal allograft rejection by 18F-FDG PET to monitor treatment efficiency. J Nucl Med. 2010; 51 :1644–1652. DOI: 10.2967/jnumed.110.078550 [PubMed: 20847180]
152. Reuter S, et al. Non-invasive imaging of acute renal allograft rejection in rats using small animal F-FDG-PET. PLoS One. 2009; 4 e5296 doi: 10.1371/journal.pone.0005296 [PubMed: 19390685]
153. Grabner A, et al. Non-invasive imaging of acute allograft rejection after rat renal transplantation using 18F-FDG PET. J Vis Exp. 2013; e4240 doi: 10.3791/4240 [PubMed: 23644348]

Europe PMC Funders Author Manuscripts

Key points

- Today, nephrology relies on the analysis of glomerular filtration rate, urinary sediment, proteinuria, and invasive kidney biopsies to assess disease activity; molecular imaging is a more specific apporach that visualizes pathological processes within the kidneys with high accuracy.
- ^{18}F-fluoro-2-deoxyglucose-PET is currently the most commonly used approach of molecular kidney imaging, although it does not reflect a specific disease or pathway.
- Most clinical trials of molecular kidney imaging are performed in patients with renal cell carcinomas and promising targets include carbonic anhydrase 9 and prostate-specific membrane antigen.
- Molecular imaging of the kidneys is challenging because it is a major elimination organ and unspecific probe uptake can be high; however, preclinical experiments and early clinical studies have identified targets and established imaging protocols for molecular imaging of acute and chronic kidney diseases, with a focus on acute epithelial or endothelial cell injury, inflammation or fibrosis.
- Similar to oncology, molecular kidney imaging might improve disease staging, prognostication, monitoring of treatment responses and patient management.

Europe PMC Funders Author Manuscripts

Glossary terms

Nanobodies
Antibody fragments in the form of a single monomeric variable antibody domain; also known as single-domain antibodies.

Aptamers
Molecules (DNA or RNA oligonucleotides). that bind with high affinity to a target molecule

Antibody- or peptide-functionalized microbubbles
Gas-filled microbubbles with a surface that is functionalized with antibodies or peptides as targeting ligands for molecular ultrasound imaging.

Extraction efficiency
A metric used to assess the elimination of an agent from the blood by comparing its arterial and venous concentrations.

Banff score
An international consensus classification for the reporting of biopsy findings from solid organ transplants.

Standardized uptake value
(SUV) A semi-quantitative measure commonly used in PET imaging for nuclide enrichment that takes into account nuclide decay, administered dose and patient weight.

Mean transit time
The average time required for a tracer to travel through a tissue.

Time–activity curve
A graph in which radioactivity is plotted against time to display kinetics of a tracer.

Europe PMC Funders Author Manuscripts

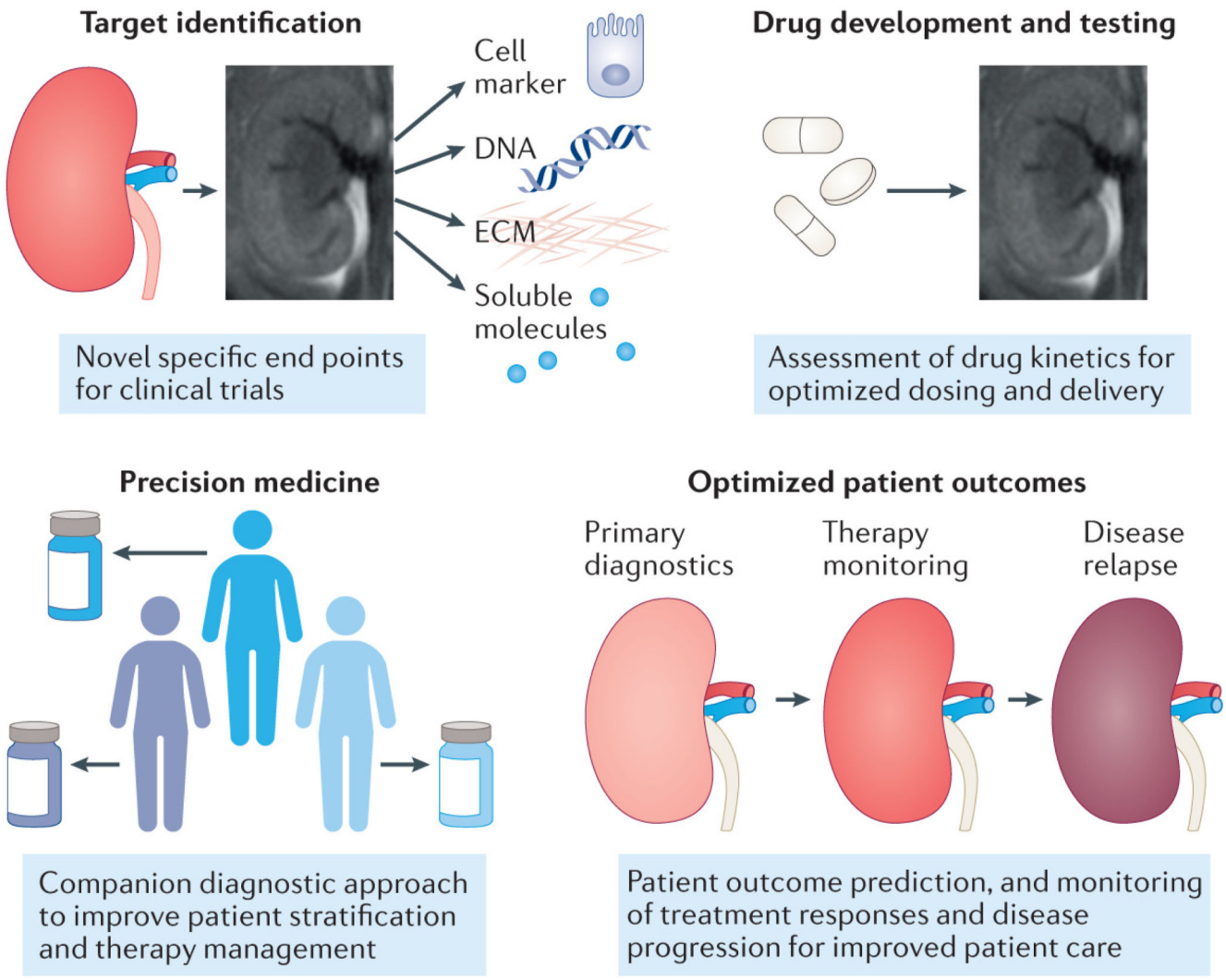

Figure 1. Categories of use and their opportunities of molecular kidney imaging

Molecular kidney imaging could be useful in four key areas of clinical research and nephrology — identification and measurement of specific targets for treatment or diagnostics; drug development and testing; precision medicine (that is, patients receive treatments that are tailored to their individual disease profile); and prediction and improvement of patient outcomes by continuous non-invasive monitoring of disease progression, remission and therapy response. The use of molecular imaging in one or more of these areas could improve diagnostics and treatment of patients with kidney disease. ECM, extracellular matrix.

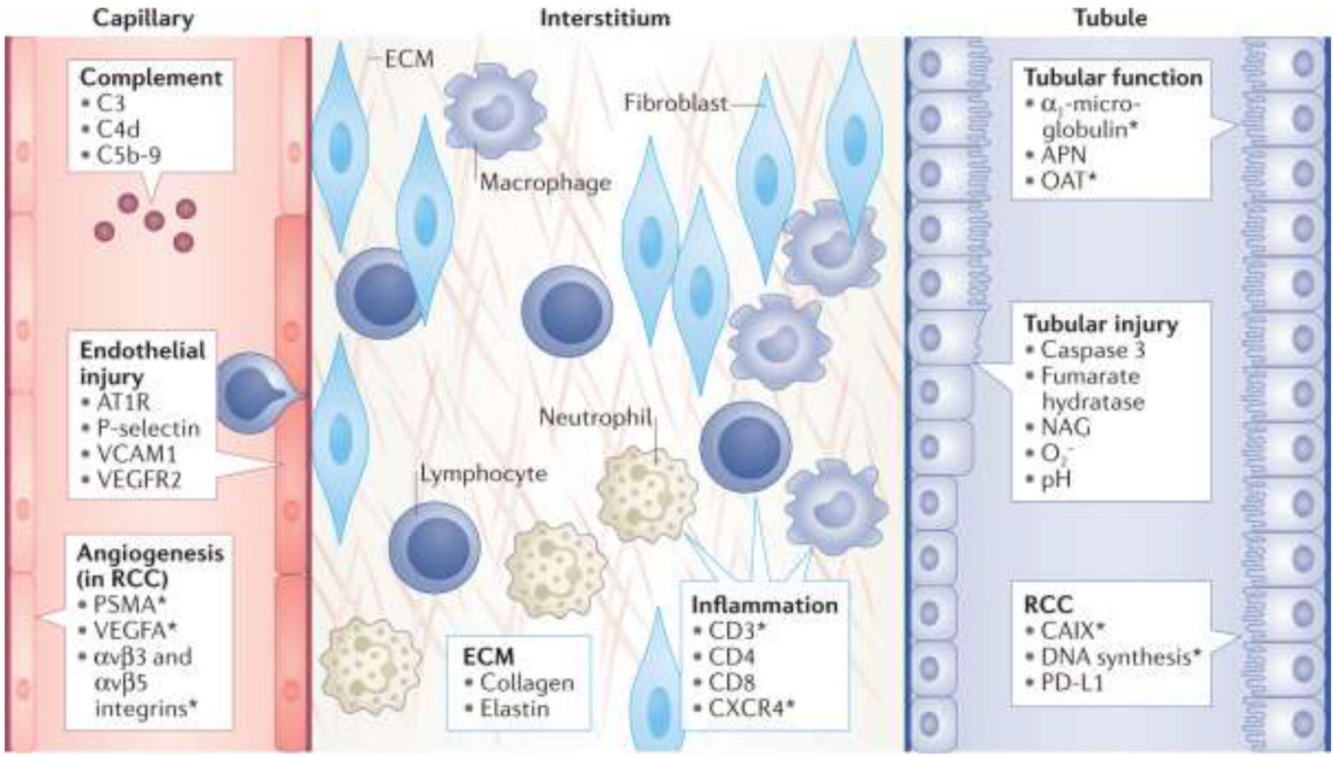

Figure 2. Targets for molecular imaging in kidney diseases

Several targets have been tested for molecular kidney imaging in preclinical and clinical studies. According to their expression, these target molecules can be assigned to tissue compartments and/or to disease pathways or mechanisms. Molecular targets in the kidney vasculature (left) comprise components of the complement system or endothelial damage markers and were used to image acute vascular injury. Proteins involved in angiogenesis have been mostly implemented to study renal cell carcinoma (RCC). Published targets in the interstitium can be divided into immune cell markers and extracellular matrix (ECM) marker that reflect inflammation and fibrosis, respectively (middle). Tubular damage (right) has either been imaged directly by using markers of injury and cell death, or indirectly by assessing changes in tubular function. Some tubular proteins have been proposed as targets for molecular imaging in RCC. APN, aminopeptidase N; AT_1R, angiotensin II type 1 receptor; CAIX, carbonic anhydrase 9; CXCR4, CXC-chemokine receptor 4; NAG, *N*-acetyl-β-D-glucosaminidase; OAT, organic anion transporter; PD-L1, programmed death-ligand 1; PSMA, prostate-specific membrane antigen; VCAM1, vascular cell adhesion molecule; VEGFA, vascular endothelial growth factor A; VEGFR2, VEGF receptor 2. *Targets tested or established in humans.

Europe PMC Funders Author Manuscripts

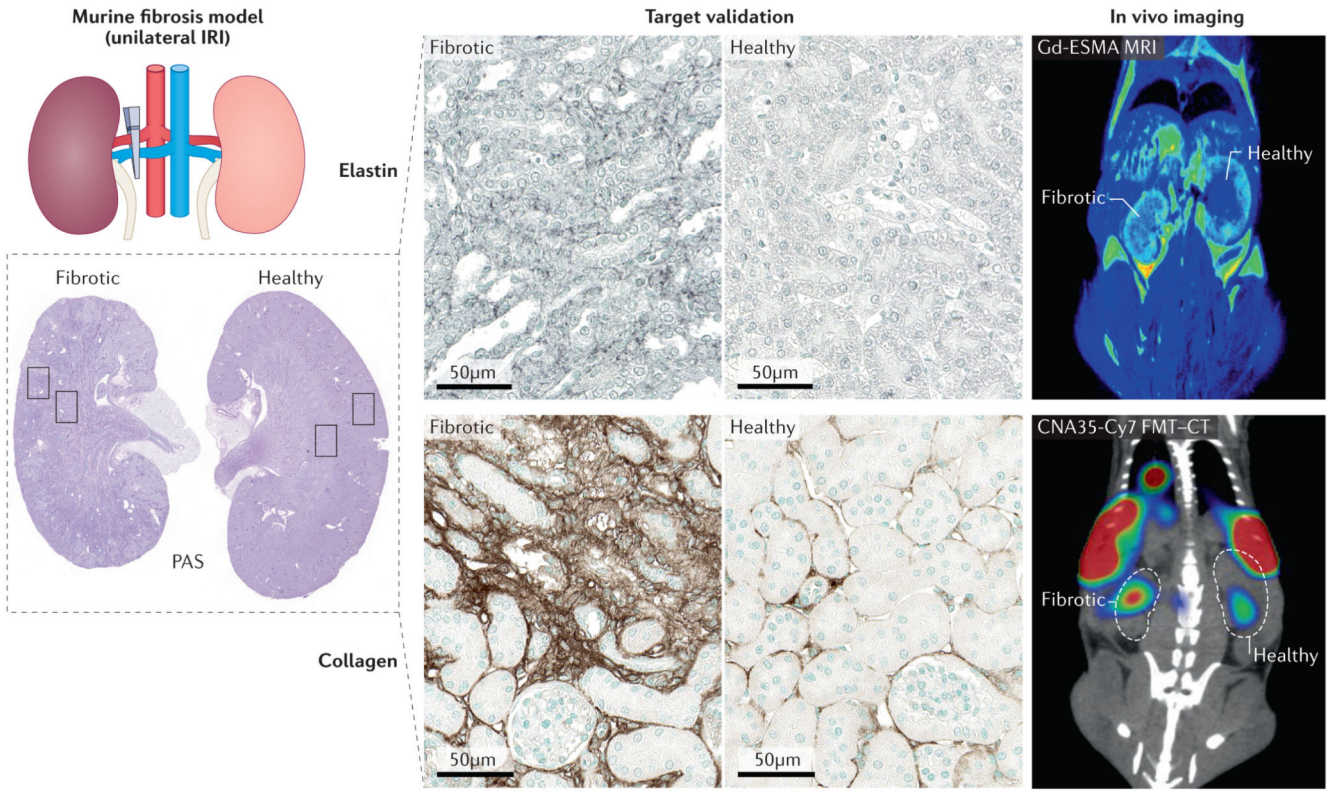

Figure 3. Examples of *in vivo* kidney fibrosis imaging in mice

Unilateral ischaemia reperfusion injury (IRI) induced fibrosis in the left kidney, as evidenced in the kidney tissue sections stained with periodic acid–Schiff (PAS) — showing shrunken parenchyme with injured and atrophic tubules, interstitial inflammation and accumulated interstitial extracellular matrix in both, cortex and medulla. Increased expression of the target proteins elastin and collagen in the fibrotic kidney compared with the healthy kidney was evident in kidney tissue sections stained with antibodies directed against elastin and collagen type I, respectively. During fibrogenesis, elastin was imaged in vivo using elastin-specific magnetic resonance imaging (MRI) contrast agent (ESMA) MRI and collagen was imaged with collagen-binding adhesion protein 35 (CNA35) fluorescence molecular tomography (FMT)–computed tomography (CT). Both approaches showed increased signal intensities in the left fibrotic kidney compared with the healthy contralateral right kidney[77,80].

Europe PMC Funders Author Manuscripts

Table 1

Advantages and disadvantages of approaches for non-invasive molecular kidney imaging.

Imaging modality	Principle of operation	Advantages	Disadvantages
Ultrasound	Based on acoustic waves (1–40 MHz) that are reflected at structure borders; the reflected echo is detected by the transducer. Probe detection relies on microbubbles (gas-filled spheres) that oscillate non-linearly during sonication and can be differentiated from the surrounding tissue.	Low patient burden (painless; no radiation) portable systems with broad availability low costs fast execution real-time images	limited tissue contrast heat development size of microbubbles only allows intravascular imaging
MRI	Based on the orientation of atomic nuclei and their spin in a magnetic field. Probes shorten the T1 and T2 relaxation times of surrounding protons and thus change the tissue contrast. For hyperpolarized imaging, the ratio of parallel to antiparallel spins is shifted resulting in an up to 10,000-fold higher signal of the injected material (although the signal is short-lived). In CEST imaging, protons that are different from the bulk water due to chemical bounds are selectively excited and fast proton exchange with the bulk water leads to a change in the water peak and, thus, a specific signal.	good resolution and tissue contrast; no radiation	time consuming examination high concentration of contrast agent required some contrast agents might have adverse effects (for example, linear Gd formulation is associated nephrogenic systemic fibrosis) absolute quantification of probe accumulation is difficult
PET	Based on radioactive substances that emit positrons (beta decay), which combine with neighbouring electrons and produce gamma rays 180 degrees in the opposite direction of each other. Gamma rays are simultaneously detected by the scanner.	low (picomolar) amounts of tracer required quantitative	does not provide anatomical information (except in hybrid imaging approaches, such as PET–CT or PET–MRI) radiation exposure high costs not broadly available
SPECT	Based on gamma-emitting radioisotopes; gamma rays are detected by a scanner rotating gamma camera.	low (picomolar) amounts of tracer required combination of tracers with different radionuclides is possible	no anatomical information (except for hybrid imaging approaches, such as SPECT–CT) radiation exposure not as sensitive or quantitative as PET
FMT[a]	Following pointwise laser excitation from different positions, the diffusely scattered light emitted from near-infrared dyes is recorded. Data are reconstructed by integrating information from the variable illumination points and the surface, absorption and scattering properties of the object.	low cost fast execution combination of tracers with different wavelength is possible suitable for preclinical studies	low tissue penetration not suitable for non-invasive imaging in patients complex image reconstruction and limited quantitative accuracy for some organs

CEST, chemical exchange saturation transfer; FMT, fluorescence molecular tomography; MHz, Mega hertz; MRI, magnetic resonance imaging; PET, positron emission tomography; SPECT, single-photon emission computed tomography.

[a] In pre-clinical studies.

Table 2

Selected clinical and preclinical molecular imaging probes and kidney targets.

Biological target	Disease or pathological process	Imaging agent	Imaging modality	Application (clinical and/or preclinical)	Refs.
Tubular function and acute kidney injury					
α1-microglobulin[a]	Tubular integrity	^{99m}Tc-DMSA	SPECT Scintigraphy	Human ;rat	15–17,49
APN	Tubular integrity	^{99m}Tc-Probestin	SPECT	Mouse	21
Caspase 3	Apoptosis	MRP3	NIR	Mouse	27
Fumarate hydratase	Necrosis	[1,4-$^{13}C_2$]fumarate	MRI	Mouse; rat	24,25
NAG	Lysosomal damage	MRP2	NIR	Mouse	27
Organic anion transporter	Tubular integrity	^{99m}Tc-MAG3	Scintigraphy	Human	50,148
		^{131}I-OIH; ^{125}I-OIH	Scintigraphy	Human	9,12
		^{99m}Tc-PAH	PET	Human	10
pH	Tubular damage	Iopamidol	MRI	Mouse	22
P-selectin	Endothelial damage	microbubbles conjugated with an anti-P-selectin antibody	Ultrasound	Mouse	32,31
		Visistar P-selectin[b]	Ultrasound	Mouse	30
superoxide anion O_2	Oxidative stress	MRP1	NIR	Mouse	27
VCAM1	Endothelial damage	Visistar VCAM1[b]	Ultrasound	Mouse	30
		VCAM-MPIO[c]	MRI	Mouse	29
Inflammation					
C5b-9	Complement activation	Ultrasmall SPIO nanoparticles[c]	MRI	Rat	45
C3b; iC3b; C3d	Complement activation	CR2-targeted SPIO nanoparticles	MRI	Mouse	43,44
GLUTs	Acute complicated pyelonephritis	^{18}F-FDG	PET	Human	35
	Cyst infection in ADPKD	^{18}F-FDG	PET	Human	36,149
	Infection caused by maintenance hemodialysis	^{18}F-FDG	PET	Human	37
Transplant rejection					
C4d	Antibody-mediated rejection and complement activation	C4d-targeted microbubbles	Ultrasound	Rat	56
$CD3^+$ T cells	Cell-mediated rejection	microbubbles conjugated with an anti-human CD3 antibody	Ultrasound	Rat	39,40
		^{99m}Tc-OKT3	Scintigraphy	Human	41
$CD4^+$T cells	Cell-mediated rejection	microbubbles conjugated with an anti-CD4 antibody	Ultrasound	Rat	39
$CD8^+$ T cells	Cell-mediated rejection	microbubbles conjugated with an anti-CD8 antibody	Ultrasound	Rat	39

Biological target	Disease or pathological process	Imaging agent	Imaging modality	Application (clinical and/or preclinical)	Refs.
CXCR4	Allograft infection after urinary tract infection	^{68}Ga-pentixafor	PET	Human	42
Fibrin thrombi	Thrombosis in acute and chronic rejection	^{131}I or ^{125}I Fibrinogen	Scintigraphy	Human	38,150
		^{99m}Tc-sulfur colloid	Scintigraphy	Human; dog	38,53–55
GLUTs	Transplant rejection	^{18}F-FDG	PET	Rat	151–153
			PET	Human	48
Granulocytes	Acute and chronic rejection	^{67}Ga-Citrate	SPECT	Human	38,53,55
Diabetes					
CD206	Mesangial expansion	^{68}Ga-IRDye800-tilmanocept	PET	Rat; mouse	66
Fumarate hydratase	Mitochondrial dysfunction and cell death	[1,4-$^{13}C_2$]fumarate	MRI	Rat	65
GLUTs	Tubular glucose transport	^{18}F-FDG	PET	Mouse	63
SGLTs and GLUTs	Tubular glucose transport	4-^{18}F-FDG	PET	Mouse	63
SGLTs	Tubular glucose transport	^{18}F-Me-4FDG	PET	Mouse	63
		^{11}C-MDG	PET	Rat	64
Chronic kidney disease and fibrosis					
Angiotensin II type 1 receptor	Hypertension	^{18}F-FPyKYNE-losartan	PET	Rat	70,71
Collagen	Fibrosis	Cy7-CNA35	NIR	Mouse	80
Elastin	Fibrosis	Gd-ESMA	MRI	Mouse	77
Renal cell carcinoma					
CAIX	ccRCC tumorgrafts	^{99m}Tc-(HE)3-ZCAIX:1-4[c] and ^{125}I-(HE)3 -ZCAIX:1-4[c]	SPECT and PET	Mouse	116
		^{64}Cu-XYIMSR-06	PET	Mouse	118
		^{111}InXYIMSR-01	SPECT	Mouse	117
	ccRCC	^{18}F-VM4-037	PET	Human	115
		^{131}I-mG250	Scintigraphy	Human	107,108
		^{131}I-cG250	Scintigraphy	Human	109–111
		^{124}I-girentuximab ^{124}I-cG250	PET	Human	112,113
GLUTs	Advanced RCC	^{18}F-FDG	PET	Human	82–89
Cell proliferation	Metastatic RCC	^{18}F-FLT	PET	Human; mouse	102–104
$\alpha_v\beta_3$ and $\alpha_v\beta_5$ integrins	ccRCC	^{18}F-fluciclatide ^{18}F-AH111585	PET	Human	124
PD-L1	ccRCC tumorgrafts	^{89}Zr-atezolizumab	PET	Mouse	125
PSMA	Metastatic RCC	^{18}F-DCFPyL[d]	PET	Human	97–100
	Primary or metastatic RCC	Glu-NH-CO-NH-Lys-(Ahx)-[^{68}Ga(HBED-CC)] [e]	PET	Human	101

Biological target	Disease or pathological process	Imaging agent	Imaging modality	Application (clinical and/or preclinical)	Refs.
VEGF-A	Metastatic RCC	[^{89}Zr]Zr-Bevacizumab	PET	Human	119,120
VEGFR2	ccRCC tumorgrafts	Visistar VEGFR2[b]	Ultrasound	Mouse	122
		Targestar[f]	Ultrasound	Mouse	123

^{18}F-FDG, 2-deoxy-2-^{18}F-fluoroglucose; 4-^{18}F-FDG, 4-deoxy-4-^{18}F-fluoroglucose; ^{18}F-Me-4FDG, α-methyl-4-fluoro-4-deoxy-D-glucopyranoside; ^{18}F-FLT, ^{18}F-fluorothymidine; ADPKD, autosomal dominant polycystic kidney disease; APN, aminopeptidase N; CAIX, carbonic anhydrase 9; ccRCC, clear cell renal cell carcinoma; cG250, chimaeric anti-CAIX antibody; ^{11}C-MDG, ^{11}C-methyl-D-gluco-side; CNA35, collagen-binding adhesion protein 35; CR2, Complement receptor type 2; CT, computed tomography; CXCR4, CXC-chemokine receptor 4; DMSA, dimercaptosuccinic acid; ESMA, elastin-specific MRI contrast agent; GLUT, facilitative glucose transporters; MAG3, mercaptoacetyltriglycine; mG250, monoclonal anti-CAIX-antibody; MPIO, microparticles of iron oxide; MRI, magnetic resonance imaging; MRP, molecular renal probe; NAG, N-acetyl-β-D-glucosaminidase; NIR, near infrared; OIH, orthoiodohippurate; OKT3, inhibitory anti-CD3 antibody; PAH, para-aminohippuric acid; PD-L1, programmed death ligand 1; PET, positron emission tomography; PSMA, prostate-specific membrane antigen; SGLT, sodium-glucose co-transporter; SPECT, single-photon emission CT; SPIO, superparamagnetic iron oxide; VCAM1, vascular cell adhesion molecule 1; VEGFA, vascular endothelial growth factor A, VEGFR2, VEGF receptor 2.

[a] Ligand for megalin and cubilin receptors.

[b] Conjugated microbubbles.

[c] Antibody-conjugated.

[d] PSMA inhibitor.

[e] PSMA ligand.

[f] Streptavidin-coated microbubbles incubated with biotinylated rat anti-mouse VEGFR2 monoclonal antibody.

Table 3

Selected PET–CT clinical trials testing molecular kidney imaging approaches.

Disease or pathological process	Imaging agent	Trial	Trial No	Status or outcome publication
Kidney transplantation	^{18}F-FDG	Observation Study for Prediction of Allograft Survival and Impact of Imaging in Kidney Transplant Recipients.	NCT03764124, https://clinicaltrials.gov/ct2/show/NCT03764124	Recruiting
RCC	^{18}F-FLT	Sunitinib Malate and Bevacizumab in Treating Patients With Kidney Cancer or Advanced Solid Malignancies	NCT01243359, https://clinicaltrials.gov/ct2/show/NCT01243359	Completed but no results published; other studies showed a detectable uptake in primary RCC[103,104]
		Sunitinib Malate in Treating Patients With Unresectable or Metastatic Kidney Cancer or Other Advanced Solid Tumors	NCT00499135, https://clinicaltrials.gov/ct2/show/NCT00499135	
	^{124}I-cG250	Pre-surgical Detection of ccRCC Using Radiolabeled G250-Antibody	NCT00606632, https://clinicaltrials.gov/ct2/show/NCT00606632	Completed; ^{124}I - girentuximab PET–CT shown to accurately and noninvasively identify ccRCC[112]
	^{18}F-VM4-037	Imaging Studies of Kidney Cancer Using ^{18}F-VM4-037	NCT01712685, https://clinicaltrials.gov/ct2/show/NCT01712685	Terminated (study was closed to accrual because imaging agent was no longer available); preliminary results indicate that the probe was well tolerated, and showed moderate signal uptake in primary tumors and good visualization of CAIX^{+}metastases[115]
	^{18}F-fluciclatide	RGD–PET–CT in Cancer Angiogenesis	NCT01492192, https://clinicaltrials.gov/ct2/show/NCT01492192	Terminated
		Reproducibility of ^{18}F Uptake by Solid Tumors Using PET Imaging Following Intravenous Administration of (^{18}F) Injection	NCT00918281, https://clinicaltrials.gov/ct2/show/study/NCT00918281	Completed; ^{18}F-fluciclatide was well tolerated and demonstrated higher uptake in chromophobe than in non-chromophobe RCC[124]
		^{18}F-Fluciclatide PET Imaging of Pazopanib Response	NCT01961583, https://clinicaltrials.gov/ct2/show/NCT01961583	Terminated (^{18}F-fluciclatide production was discontinued)
		^{18}F-Fluciclatide for Kidney Cancer Imaging Studies and Treatment	NCT01633255, https://clinicaltrials.gov/ct2/show/NCT01633255	Withdrawn
	^{18}F-DCFPyL	Study of PSMA-targeted ^{18}F-DCFPyL PET–CT in the Evaluation of Patients With Renal Cell Carcinoma	NCT02687139, https://clinicaltrials.gov/ct2/show/results/NCT02687139	Completed; ^{18}F-DCFPyL imaging can identify patients with oligo-metastatic ccRCC but yielded only inconsistent detection of other RCC subtypes [99,100]
	^{89}Zr-bevacizumab	VEGF Imaging in Renal Cell Carcinoma (Renimage)	NCT00831857, https://clinicaltrials.gov/ct2/show/NCT00831857	Completed; tumour uptake was high in metastatic RCC, with remarkable inter-patient and intra-patient variability; bevacizumab–IFNα strongly decreases tumour uptake, whereas sunitinib resulted in only a modest reduction[119]
Solid tumors: high grade gliomas; lung cancer, head and neck cancer, sarcoma, RCC and breast cancer	^{89}Zr-bevacizumab	VEGF Imaging Before and During Everolimus Treatment for Renal Cell Carcinoma (Everolimage)	NCT01028638, https://clinicaltrials.gov/ct2/show/NCT01028638	Completed; everolimus decreases tumor uptake of ^{89}Zr-Bevacizumab[120]

^{18}F-FDG, 2-deoxy-2-^{18}F-fluoroglucose; ^{18}F-FLT, ^{18}F-fluorothymidine; CAIX, carbonic anhydrase 9; ccRCC, clear cell renal cell carcinoma; cG250, chimaeric anti-CAIX antibody; CT, computed tomography; IFNα, interferon α; PET, positron emission tomography; PSMA, prostate-specific membrane antigen; VEGF, vascular endothelial growth factor.

Europe PMC Funders Author Manuscripts